Photoacoustic Infrared Spectroscopy of Thin Polyimide Layers on Glass Substrates

NISTIR 6097

Photoacoustic Infrared Spectroscopy of Thin Polyimide Layers on Glass Substrates

Brian Dickens
Polymers Division
Materials Science and Engineering Laboratory
National Institute of Standards and Technology

December 1997

U.S. DEPARTMENT OF COMMERCE
William M. Daley, Secretary

TECHNOLOGY ADMINISTRATION
Gary R. Bachula, Acting Under Secretary for Technology

NATIONAL INSTITUTE OF STANDARDS AND TECHNOLOGY
Raymond G. Kammer, Director

NISTIR 6097

Table of Contents

Photoacoustic Infrared Spectroscopy of Thin Polyimide Layers on Glass Substrates

Brian Dickens

Polymers Division
National Institute of Standards and Technology
Gaithersburg, MD 20899

Abstract

Three commercially-available polyamic acid solutions were deposited on small glass substrates, cured in nitrogen or air by heating at 2 °C/min or 20 °C/minute to 350 °C, and cooled over 16 h. Most of the resultant polyimide layers were 8 μm to 13 μm thick. The cured layers were examined on their substrates using photoacoustic spectroscopy (PAS) in step-scan, time-sliced mode, where each spectrum contains time-weighted contributions from different depths in the layer. The three polyimides can easily be distinguished from one another using only the most intense spectrum from a set of timed-delayed spectra. Differences in polyimide layer thickness on the glass substrate are evident. The presence of bi-layers can be discerned. Effects of oxidation were observed. Two of the polyimides, characterized as semi-flexible and semi-rigid, tend to order physically when cured on a substrate. Birefringence measurements suggested that each polyimide had its own degree of order, but the amount of order did not change significantly for the various specimens of a given polyimide. X-ray wide angle diffraction and photoacoustic spectra also suggested no difference in order for a given polyimide. A correlation algorithm was used to quantify differences between sets of time-weighted spectra from different specimens. The algorithm used all the timed-delayed spectra in a set except one or two of the weakest and indicates whether (but not how) two specimens differ over their "thermal depths". However, the complete set of time-delayed spectra provided no new information over that found in the most intense spectrum.

Introduction

Polymers are widely used in electronic packaging to provide low-dielectric-constant layers that insulate the metal conductors. The material used in the layer should: 1) initially be tractable (i.e., soluble in some suitable solvent) so that the layer can be deposited on a substrate, 2) cure to become inert to the solvents and conditions used in the depositing of successive layers, 3) adhere to the substrate, to previously-deposited inert layers, and to the metal conductors, 4) have a range of thermal expansion coefficients, conferred by anisotropy in the film, so that adhesion to dissimilar materials such as substrate and metal conductors can be accommodated over a range of temperatures, 5) be strippable if reworking is necessary, 6) planarize rough structures, 7) be stable at temperatures which allow soldering to be carried out, and 8) be relatively unaffected by environmental factors such as humidity.

For various reasons, polyimides have generally been used in these layers. The polyimides have traditionally been formed *in situ* from soluble precursors containing ionic (amic acid) or labile (amic ester) groups. On being heated, the precursor loses solvent and forms chemical bonds of the imide type. The polyimides used in electronic packaging are designed to contain aromatic structures because aromatic polyimides are insoluble and thermally stable. The insolubility of the polyimide allows subsequent layers of precursor to be deposited and the thermal stability allows the package to be heated to soldering temperatures. Rigid imide/aromatic ring structures have the potential for preferred orientation, for example lying parallel to one another, which confers anisotropic expansion.

The cure of a precursor to a polyimide thus entails chemical changes which render a soluble material insoluble and heat-resistant. The chemical cure continues until, as a result of the formation of large rigid structures, the remaining reactive groups are no longer mobile enough to be able to interact with one another. In non-flexible polyimides, physical ordering may also take place to the extent permitted by the mobility of the polyimide moieties. The cure process does not attain equilibrium. The state achieved depends on the precursor itself, its concentration in the solvent, the extent to which the precursor and the solvent react with one another, the rate of loss of solvent and low molecular weight reaction products (of which water is typically one), and the time spent at each temperature of the cure cycle.

Although the limits on the properties of a polyimide are governed by its chemical composition, the state of cure determines the extent to which these properties are realized. If polyimide layers are to be cured in a reproducible way, the state of the cure (the net result of the degree of chemical reaction, the extent of ordering and the layer thickness) should be monitored. Assessments of cure should follow chemical and physical transformation in layers 5 μm to 25 μm thick and should be affected by variations in degree of chemical cure and physical ordering with depth in the layer.

The first consideration is to use techniques which are as specific as possible, i.e., techniques that indicate reactant and product groups and degree of order, rather than techniques which measure properties affected by the cure and order parameters. For chemical changes, infra-red (IR)

spectroscopy has traditionally been invaluable in following which groups appear and disappear and in estimating rates of reactions, although overlaps of absorbances in the spectrum frequently occur and obscure details. IR techniques are rarely precise enough to allow discrimination between 99% and 100% reaction or 0% and 1% presence of components, but on balance are worth examining. Order in the solid state is typically studied by diffraction techniques and can be followed by birefringence. To some extent, IR can also be used to infer the existence of orientation from differences in intensities of absorption in chemically identical systems.

Depth profiling (see, for example, reference 2) over more than a few micrometers is difficult to carry out non-destructively. Depth profiling using IR is possible with attenuated total reflectance (ATR) to depths of 1 μm to 10 μm, depending on the wavelength and the angle of incidence of the probing radiation. The depth examined with ATR varies across the IR spectrum and there is generally not exact correlation between absorbance and the concentration of absorbing species. Ratios or correlation curves are used [2]. Much greater depths, at least 25 μm in favorable cases, can be attained with photoacoustic spectroscopy (PAS). Recent advances in PAS allow the depth profiling to be uniform across the spectrum.

Techniques which are secondary in terms of monitoring cure and ordering include dielectric measurements and fluorescence. Dielectric measurements are expected to be more precise than IR measurements when ionic groups are in very low concentration but are crippled by the presence of ions and some impurities. Fluorescence measurements must be related to the chemical groups involved in the fluorescence and may be quenched by atmospheric oxygen or dominated by impurities.

This investigation examines the utility of PAS in characterizing polyimide layers on a substrate. PAS is fairly rapid, non-destructive, and requires minimal sample preparation, but its interpretation is neither simple nor straightforward.

There are basically four methods of applying a polyimide layer to a substrate. The first method is to attach an already cured film to the substrate. The second is to cast a soluble polyimide from solution. In these two cases, the cure of the film can be measured beforehand. If the polyimide has been cast, the orientation will have to be measured. The third method is to form the polyimide groups after deposition on the substrate, as in the "traditional" conversion of polyamic acid to polyimide by heating. The fourth way is to preform the polyimide groups in relatively small molecules but to add to the molecule other reactive groups which on curing will produce crosslinking.

We have applied PAS to the study of polyimide layers produced by heating polyamic acids, the third of the four methods described above. This is a widespread way of producing polyimides in electronic packaging.

Photoacoustic Spectroscopy (PAS)
PAS was first discovered by Alexander Bell [3], was subsequently neglected, and was revived in

the 1970's by Rosencwaig [4] when sensitive microphones became readily available. Further developments in the theory were provided by several investigators [5-8]. In the PAS technique, polychromatic radiation is pulsed onto the specimen. The radiation enters the specimen and is absorbed at wavelengths and to degrees characterized by the absorption spectrum of the material. Where radiation is absorbed, heat is generated. The heat diffuses in the specimen and the heat which arrives at the specimen surface heats up the ambient gas, typically helium. A small expansion of the gas is produced and the resultant pressure is registered by a microphone.

The slow diffusion of heat allows depth profiling to be carried out by varying the pulse rate of the radiation. Pulsing the radiation more rapidly leaves less time for the heat to diffuse to the specimen surface before more heat is generated and examines a shallower layer of the specimen. The pulsed radiation is usually produced using the interferometric aspect of FTIR, which has been found to give better signal/noise ratios than mechanical or electronic chopping of the incident beam [9]. In typical FTIR spectroscopy, a smoothly moving mirror continuously changes the path length in one of the two parts of a split beam. When the beams are recombined, the path length difference produces interference between the beam components. The rates (modulation frequencies) at which these interferences occur depend on the mirror velocity and the wavelength of the component of the beam. In conventional FTIR spectroscopy, the mirror moves with constant velocity in a given scan. Thus, the modulation frequency varies inversely with wavelength across the spectrum, which in turn makes the depth profiled by PAS vary across the spectrum. It is then difficult to interpret the resulting PA spectra in terms of depth in the specimen.

One advance in PAS is to step the FTIR path length difference to a new value instead of smoothly varying it [9]. This abruptly changes the intensities of all the components in the recombined beam incident on the specimen. Modulation of the intensity of the components in the incident radiation is achieved by "dithering" one of the mirrors to produce a path length change which is less than any IR wavelength of interest. Thus, no component of the IR spectrum extinguishes more frequently than any other and the same modulation frequency occurs across the spectrum. Depth profiling is then uniform across the spectral range. Also, because the modulation frequency is determined by the rate of dithering the mirror, PAS studies can use higher frequency regions, such as the near IR, which in a smoothly-moving mirror system modulate too quickly for the detector system to handle.

A second advance is the monitoring of the arrival of heat as a function of the position of the mirror in the dither cycle. The signal seen by the detector is the sum of the heat generated at the surface of the specimen, the heat generated an instant previously in the sub-surface region, the heat generated still earlier in the depth of the layer, and so on. Time-slicing the detector response as a function of the time from when the mirror went through its zero position in the dither cycle allows each depth in the specimen to have a different contribution to the signal as the dither proceeds. In this investigation, PA spectra were measured at 20 positions in one half of the dither cycle.

Estimation of Thermal Depth of a Polyimide Layer

PAS is considered to probe a specimen down to its thermal depth (or thermal length), the depth from which the heat diffusing to the surface is damped by $1/e$. The thermal depth is defined as $\mu = \sqrt{[2\kappa/(\rho C_p \nu)]}$, where typical values from the manufacturer's literature for the polyimides used here are: thermal conductivity $(\kappa) = 0.0016$ J cm^{-1} s^{-1} °C^{-1}, density $(\rho) = 1.45$ g cm^{-3}, and specific heat $(C_p) = 1.1$ J g^{-1} °C^{-1}. For a dither frequency (ν) of 400 Hz, the thermal depth of the polyimide is then $\mu = 22$ μm.

Phased-Modulated (Time-Sliced) PAS Spectra

The flux of monochromatic radiation incident on a specimen layer is attenuated according to

$$-dI = I_x \alpha_x dx$$

as the beam passes through a section dx of the specimen. I_x is the flux at depth x, and α_x is the absorbance per unit thickness of section dx. The flux at depth x in a non-homogeneous material is related to the flux, I_0, incident on the surface of the layer by

$$I_x = I_0 (1-R) e^{\int -\alpha_x dx}$$

where R is the fraction of the incident radiation which is reflected externally at the surface of the material. The heat evolved at depth x by thickness dx is given by -dI. For polychromatic radiation, that part, $E_{x\lambda}$, of the heat generated at depth x in thickness dx from radiation of wavelength λ and which is emitted from the front surface of the layer by diffusion is given by

$$E_{x_\lambda} = -dI_{x_\lambda} (1-R_T) e^{-x/\mu} = I_{0_\lambda} (1-R_\lambda)(1-R_T) \alpha_x e^{\int -\alpha_{x_\lambda} dx} e^{-x/\mu} dx \tag{1}$$

where R_T is the fraction of the thermal wave reflected internally at the layer/air surface and μ is the thermal depth of the layer. R_λ is the fraction of incident radiation reflected externally for wavelength λ. Because μ depends on the square root of the thermal conductivity, which in turn depends markedly on the composition and molecular orientation of the material, μ is a function of x for a non-homogeneous material. Also, the absorptivity $\alpha_{x\lambda}$ of a non-homogeneous specimen is a function of depth as well as of wavelength. Dependency of absorptivity and thermal depth on composition and state of orientation prevents the deconvolution of the PAS signal into contributions from individual layers in non-homogeneous specimens.

The total emission of heat is obtained by summing $E_{x\lambda}$ over all depths in the layer and all wavelengths in the incident radiation to give the detector signal D_s for step s in the step-scan sequences. The set of D_s measurements, D, obtained as the path difference in the FTIR system is stepped through s steps, constitutes the FTIR interferogram. Deconvolution of D as a function of wavelength to give the absorption spectrum in a dithered step-scan mode is achieved by correcting for several phase shifts and relating modulations in D to modulations of the components of the incident beam brought about by the changing path difference [15]. This

process of producing a spectrum S from each set of D_s measurements is the normal mode of operation for FTIR, regardless of whether the path difference is varied smoothly or stepped discretely.

Time-delayed Photoacoustic Spectra of Polyimide Layers

When all detector measurements are taken at a given point in the dither cycle instead of being summed over the entire cycle, the spectrum so obtained may be labelled S_t to denote that it was taken at time t in the dither cycle. The absorption $S_{\lambda t}$ (at wavelength λ in time-delayed spectrum t) represents the summation of the heat generated by absorption of radiation of wavelength λ and emitted from the surface section of the layer at time t, the heat from the next section down in the layer generated at time $t-\delta t$ but only now arriving at the surface, and in general the heat from the nth section of the layer generated at time $t-n^2\delta t$. The $n^2\delta t$ values are related to distance into the layer through the thermal diffusivity of the layer. Heat may be considered to be generated simultaneously in the various sections of the layer by the absorption of radiation of wavelength λ because the velocity of the incident radiation in the material is much higher than the velocity of diffusion of the generated heat. Thus, the heat sources are all in phase as the heat is generated, but the phase of the generation of heat as seen at the surface of the specimen by the detector microphone systematically changes with depth in the layer. In deconvoluting the heat components, many phase considerations come into play [15]. Treating the phases correctly is a major problem even for homogeneous materials [11].

For very high absorptions, only the surface region of the specimen contributes to the spectrum. Because depth in the specimen plays no part, the time-delayed behavior of the very high absorptions indicates directly the intensity of the incident radiation as it varies in the dither cycle.

The weakest absorptions probe the layer down to near its thermal depth. Absorptions of intermediate strength probe the specimen down to intermediate depths; the region probed is then limited more by the intensity of the radiation than by its modulation frequency. Layers composed of two materials with radically different absorption spectra have peaks present only in some of the time-delayed spectra (where the absorption of the underlying part is high and the absorption of the surface part is low - see for example, reference 13). In simple cases such as a homogeneous top layer which is thermally thin with optical windows (i.e., spectral regions where radiation is not absorbed) and a homogeneous bottom layer which is *thermally thick and considerably different in chemical composition from the top layer*, measuring two spectra separated by 90° in phase in the dither cycle may suffice to separate the contributions from the two layers [10,13].

Although the result of curing a polyamic acid to an anisotropic polyimide is not usually a homogeneous system, inspection of the PAS polyimide spectra in Figure 1 shows that all absorptions more or less change together with the time slicing. The conclusion is that the gross features of the layer are quite similar throughout the layer. The contribution of the sub-surface part of the layer to the signal decreases markedly with depth in the specimen because of the two exponential damping factors in Equation 1. Deconvolution effectively requires scaling the depth

contributions by functions of the absorptivity and thermal diffusivity at each depth, although these parameters are not well known. Therefore, attempts to deconvolute the effects of the subsurface part of the layer from the effect of the surface are ill-advised.

An additional consideration is the precision to which the spectra can be measured. In the case of a somewhat homogeneous layer, the spectrum of the surface is dominant because the surface receives the most radiation and its heat emission is not damped. The effect of the sub-surface layers is a small perturbation on the spectrum obtained from the surface of the layer (there are no optical windows). The measurement of a spectrum is affected by such factors as the effective incident power at each wavelength, the atmosphere in the PA cell, and the extent to which the dither frequency and the step frequency can be demodulated from one another. The cell is purged with helium to maximize the effect of the emitted heat and to move the cell resonance to higher frequency so that it will not affect the measurement of the spectrum. Any loss in this purge or evolution of absorbed gas by the specimen may significantly change the intensity of the spectrum vis-a-vis other spectra in the series of time-resolved spectra. Such effects are sometimes seen in PAS spectra, even if care is taken to purge the cell periodically. The contribution of the sub-surface part is therefore not well known.

Fortunately, it may be possible to circumvent the necessity for deconvolution, although one can not circumvent a natural loss of sensitivity with increasing depth in the layer. A finger-print of a specimen can be produced from a study of detector response as a function of time delay at *selected wavelengths* (a series of slices through Figure 1). The wavelengths selected must of course penetrate to the appropriate depth in the specimen and the spectral absorptions must be influenced by the polyimide parameters of interest.

In the Experimental Section, sets of "slices" through time-resolved spectra of polyimides have been compared quantitatively. The slices are obtained by arranging the spectra according to their times in the dither cycle, with zero delay in the center and the longest delay repeated at each end. Each slice is a sequence of absorptions, one from each spectrum, at a given wavelength. The "peak-like" appearance of the slice is very convenient for visual comparisons. Taking slices at several wavelengths gives a set of slices which may then be compared with a corresponding set from another specimen.

Experimental

Three solutions of commercially available polyamic acids were obtained from DuPont de Nemours, Inc. [14]. Chemical formulae of the polyamic acids and their correspondence to the DuPont designations are shown in Figure 2. Attempts were first made to spin films on pieces of glass which were then cut to 7 mm square for the PAS cell. The films flaked off the glass during the cutting process. Films were then made directly on 7 mm squares of glass. A drop of polyamic acid solution was placed on the stationary glass plate, spun as indicated in Table I, and cured as indicated in Table II. Estimates of the thicknesses of the polyimide layers were obtained using a micrometer but these measurements did not appear to be precise because they did not correspond to those expected from spin-casting. Long after all PAS measurements had been

completed, a Metricon model 2010 dual-wavelength prism-coupler thickness-measurement system [14] became available. The finding that the prism coupler was unable to make contact with the layer surfaces when the polyimides were still on the glass substrates revealed the existence of depressions in the centers of the polyimide surfaces. The polyimide layers were removed from the glass plates by soaking in water. It was then possible to obtain estimates of the thickness of their centers using the Metricon. These thickness values and the associated estimates of the refractive index are given in Table I as "center". The thicknesses measured with the micrometer are given in Table I as "rim". Comparison of the refractive indices for the mutually perpendicular TE and TM cases allows one to estimate the anisotropy in the polyimides from the birefringence but it must be borne in mind that the birefringence is very dependent on layer thickness [16].

For the photoacoustic measurements, a Bio-Rad FTS 60A-896 FTIR spectrometer [14] was used in step-scan mode. An MTEC 200 photoacoustic cell [14] was employed. Brass slugs were used to bring the specimen to about 1 mm from the cell window to maximize the signal. The FTIR mirror system was stepped at 50 Hz. Each step produces a different mix of intensities for the components of the incident beam. Interferogram data were measured at 8 cm^{-1} resolution in "co-averaged" mode at 4000 steps per scan, i.e., 2000 steps on each side of the center-burst. At each step, the mirror system was "dithered" with an amplitude of 2 He/Ne fringes from the stepped position using a dithering frequency of 400 Hz. 400 Hz was chosen from an available range of 0.004 Hz to 800 Hz because it was appropriate for the intended (20 μm) specimen thicknesses. The spectra used in this investigation result from averaging two scans. Collecting data for more than two scans per spectrum or obtaining multiple spectra for statistical analysis was deemed too time-consuming for the exploratory nature of the study. So-called "phase-modulation" (i.e., time-delayed) spectra were taken at 20 fixed and equally spaced intervals in the dither cycle using a lock-in amplifier (demodulator) supplied by Bio-Rad [14] as an accessory to the FTS 60A.

The energy spectrum of "useful" IR radiation (Figure 3) incident at each time delay in the dither cycle was estimated from the PA spectra of a completely absorbing body - a black rubber pellet supplied by John McClelland of MTEC [14] and used as recommended by R.O. Carter et al. [17]. The intensity distribution in the energy spectrum results from the combined effects of the beam-splitter in the FTIR spectrometer and the dither amplitude. The amplitude of a shorter wavelength component of the incident beam varies more widely in the dither cycle than that of a longer wavelength because the displacement in the dither is a bigger fraction of a shorter wavelength. From Figure 3, the best discrimination for the conditions used is seen to be at about 2800 cm^{-1}.

After the black rubber spectra had been taken, similar spectra were obtained for the various polyimide/glass plate specimens. The polyimide spectra were normalized by dividing them by the black rubber spectrum for that time slice. Figure 1 contains time-delayed spectra arranged so that the most intense absorptions change from lowest intensity (at one extreme of the dither excursion) through the highest intensity (at the center of the dither range) to the lowest

intensity at the other extreme of the dither cycle. The spectra are from a layer of PI 2525 on glass. Because the layer shows only small variations in composition and orientation, the highest absorption serves to define the zero delay in these spectra.

Comparison of the PA Spectra
Several authors [18,19] have shown where the IR spectrum shows information on the process of thermally curing polyamic acids to form polyimides. Many of these changes involve the carbonyl group of the imide ring and take place at intensely-absorbing parts of the spectrum. For example, the carbonyl absorptions at about 1720 cm^{-1} in Figure 1 have an intensity of about 1.8.

Depth profiling to the thermal depth can only be carried out using the weakly absorbing parts of the PA spectrum. For 1/e of the incident beam to remain after traversing 22 µm of absorbing material (i.e., the thermal depth of a polyimide layer under the conditions used here), the absorption per micrometer, A, in $I=I_0 10^{-Ax}$ must be 0.02; I_0 is the incident flux and I is the flux at depth x. The carbonyl absorption may be used as an internal standard to select absorptions potentially suitable for use as internal probes. Pryde [18] measured 1.6 for the carbonyl absorption in a 2 µm thick polyimide film. This suggests that, to probe about 20 µm into a polyimide layer, one has to use absorptions which are (100x0.02/0.8)=2.5% or less of the carbonyl absorption (0.8 /µm) at 1720 cm^{-1}. Thus, the analysis would be limited to absorptions which are about 0.05 or so in Figure 1. Several such places in the polyimide spectra are given in Table III and were used to generate the slice information in Figure 4. Most of these spectral locations are not in the well-measured part of the spectrum - the places of appreciable intensity in Figure 2. A few such places have been included, either as valleys (1554 cm^{-1}) between intense spectral absorptions or as small undulations on the side of or near (1850 cm^{-1} to 1900 cm^{-1}) the carbonyl peak at 1780 cm^{-1}. If appropriate spectral regions have already been identified, the beam-splitter and dither amplitude should be chosen to provide adequate discrimination (see Figure 3) in that region.

Tests showed the reproducibility of the PAS process to be good. The "peaks" in Figure 4 are the absorptions in five sets of slices through time-delayed spectra at the wavenumbers given in Table III. Wavenumbers identifying the slices are given along the abscissa in Figure 4. The spectra were arranged with the zero delay in the center and with the longest delay repeated at both ends. Each "peak" is a slice through a set of 20 time-delayed spectra. A series of such peaks constitutes a PAS signature and, because the maximum absorption is quite small, presumably contains contributions from depths down to about the thermal depth. For visual purposes, all slices in the Figures have been normalized to give equal intensity for the absorption at 1554 cm^{-1}, which is a valley next to the aromatic breathing mode.

Total thicknesses of the PI layers on glass
The slices in Figure 4 were taken through the PA spectra of three specimens of PI 2525 and two specimens of PI 2545, all on glass. Two effects are evident: the mismatch of the spectra at 978 cm^{-1} and below (at A in Figure 4) and the clear separation of the spectra into two classes (one from PI 2525 and the other from PI 2545) at 1852 cm^{-1} (B in Figure 4).

When the optical measurements of layer thickness revealed that the centers of the PI layers were unexpectedly much thinner than the edges, it became clear that the center thicknesses of the specimens, where the PAS spectra were measured, were about half the thermal lengths of the polyimide layers and that the spectra include considerable contributions from the IR absorption of the surface of the glass substrate. Figure 5 compares spectra of the glass substrate and a typical polyimide and shows that the glass is more absorbing than the polyimide near A in Figure 4. Figure 6 compares spectra for the center and extreme of the dither cycle for the glass substrate and shows that the glass contributes unevenly to the center and extreme spectra. Subtracting the glass spectra from the composite PI/glass spectra is not a simple task.

The 978 cm^{-1} slice in Figure 4 is shown in the left hand side of Figure 7. The central peak in Figure 7 was used to correlate the slices to one another so they can be compared visually. The highest absorption at 978 cm^{-1} is from specimen 20, which therefore contains the largest contribution from the underlying glass and must be the thinnest of the three PI 2525 specimens 19, 20 and 39. The next two highest absorptions are from specimens 19 and 39, which are seen to be comparable in thickness but thicker than specimen 20. The lowest absorption at 978 cm^{-1} is from specimen 34, which is therefore the thicker PI 2545 layer. The next lowest absorption is from specimen 22, which is therefore thinner than 34. These interpretations are in agreement with the center thicknesses in Table I.

Comparison of bilayers with the pure materials
The remaining absorptions in Figure 7 are from specimens 45, 46 and 47, which are two-layer specimens made from PI 2545 on PI 2525. The relative contributions of PI 2525 and PI 2545 can be assessed from absorptions such as at 1852 cm^{-1} (the right-most slice in Figure 7), where slices from the spectra of the double-layer specimens 45, 46 and 47 are compared with similar slices from the pure materials.

To compare thicknesses and degrees of chemical similarity of thermally-thin PI films on glass, one could therefore use the region of the spectrum below 1500 cm^{-1}, where the contribution of the glass to the PAS spectra is at its maximum. The various layer thicknesses in the specimens used here have been shown to be definitely not identical and have been ranked qualitatively in order of thickness. The process also distinguishes between homogeneous layers and double layers (Figure 7).

Since it was fortuitous that the compositional aspects of the bi-layer specimens were visible using the arbitrarily-selected weaker absorptions given in Table III, a search was made for spectral regions which would demonstrate the effect more clearly. A small computer program was used to identify where the PI 2525 and PI 2545 spectra differ by 50% where the absorbance of the glass is the least, i.e., between 1800 cm^{-1} and 3500 cm^{-1} and less than 800 cm^{-1}. Comparison of various low-absorbance slices in these regions (including C and D in Figure 8) revealed that the glass still had too great an influence on the spectra because the PI absorptions were too weak. The C-H absorbances at D in Figure 8 are in agreement with the order of *total* thicknesses given

for the bilayers in Table IV.

Attention was then turned to the more intense regions of the spectra, where the polyimide dominates the spectrum. Figure 8 contains PA spectra from the center of the dither cycle for specimens of PI 2525, PI 2545 and the bilayers. These spectra are very similar but can be distinguished from one another at E, F and G in Figure 8. Parts F and G of the spectrum are shown in more detail in Figure 9. The spectra in both Figures have been normalized to the aromatic breathing mode peak at 1504 cm^{-1}. The contributions of the various depths in the specimens to the spectra in Figure 9 are weighted by functions of the absorptivity and the depth in the layer (Equation 1). At the most intense part of the spectra (F in Figure 9), all the bilayer spectra coincide with those of PI 2545, the polyimide in the upper layer. At G in Figure 9, the top layer (PI 2545) absorbs much less than the underlayer (PI 2525), which therefore dominates the spectra. The bilayer spectra lie between those of the underlayer and the overlayer, as expected, with specimen 45 lying closer to the underlayer, 47 lying closer to the overlayer. Specimen 46 lies between specimens 45 and 47. The degree of correspondence between the spectra of the bilayers and the underlayer is in agreement with the thicknesses of the underlayers in the bilayer specimens.

It was deemed wise to check other regions of the spectra to see how these compositional effects change with total depth probed and total radiation absorbed. At H in Figure 9, where the underlayer and overlayer have the same trend of absorptivity with wavenumber, all spectra change together and the interpretation is not visually obvious. Also, the lower absorbance of the polyimides allows the underlying glass to contribute to the spectra. Three ranges of absorbance are compared in Figure 10. Figure 10c contains the central part of Figure 9 and is shown so that the scales of the absorbances can readily be seen. Figures 10a and 10b are other regions in the spectra where the absorbances of PI 2525 and PI 2545 differ. However, these absorbances do not differ enough in Figure 10a to exert much effect on the spectra of the bilayers, and the situation in Figure 10b is no better. Some influence is seen in the width of the peaks at the left hand side of Figure 10a, but these effects are very tenuous. *The absorbances are simply not high enough to exert a large effect on the spectra.*

These findings shed some light on where to slice the spectra when variations with depth in the specimens are to be examined. If total thicknesses of the polyimide films are important, then slices should be taken at both intense and relatively weak absorbances. If compositional effects in the top (say) 10 μm are of interest, then only the more intense absorbances should be used. The minimum depth probed by modulation alone is about 15 μm using the step-scan/dither approach because the highest available dither frequency is 800 Hz. In non-step scans, the depth profiled is shallower but is not uniform across the spectrum. In attacking an unknown case, the sensitive regions of the spectrum are not known in advance and may prove difficult to identify.

Effect of air on the cure
Tests were carried out to see if other aspects of the cure could be monitored using step-scan PAS. PA spectra from the center of the dither cycle (where the contribution from the surface is at its

maximum and contribution from the substrate is at its minimum) from PI 2525, PI 2545 and PI 2611 cured at 2°C/min and 20°C/min in N_2 and at 2°C/min in air are shown in Figures 11 to 13.

For PI 2525 cured in air, there is a little less absorbance from the imide group at the arrows in Figure 11. There is no discernible effect of cure speed.

The comparison for PI 2545 (Figure 12) reveals a similar discernible effect of air on the cure, although less than was the case for PI 2525, and very little if any effect of cure speed under the conditions used here.

For PI 2611 (Figure 13), there is a very small effect of air on the cure and a hint of an effect of cure speed, although any such effect is very small and may also have resulted from differing layer thicknesses.

Quantitative Comparison Index

For automated judgements such as on-line control, measurements must often be quantified and condensed into an index, although this obviously implies a loss of detail. One way to proceed in the case of spectra is to provide quantitative estimates of mismatch between spectra or between spectral slices. A cross-correlation algorithm (see, for example, reference 20) to produce quantitative comparisons of curves such as chromatograms was described in reference 21. The procedure was used to calculate a "match" factor M_{ij} between curves A_i and A_j from

$$M_{ij} = [\sum A_i A_j - (\sum A_i \sum A_j)/n]^2 / \{[\sum A_i^2 - (\sum A_i \sum A_i)/n][\sum A_j^2 - (\sum A_j \sum A_j)/n]\}.$$

This match factor removes the effect of scaling and therefore matches the *shapes* of two curves. The same procedure can be applied to parts of the PA spectra, for example to the spectra from the center of the dither cycle and to sets of slices through the time-delayed PA spectra where the slices are sets of PA absorbances, each at a given wavenumber, sampled regularly throughout the dither cycle. The choice of where to examine the spectra is clearly critical. If spectra themselves are to be compared then a series of individual absorbances or short ranges from the spectra should be used. If assessments over depth in the layer are required, then slices can be taken at pre-selected frequencies. Since only the shapes of the curves are compared and the scales of the curves have no effect, each component of the match must include a "normal" region which will in effect define the scale. Very importantly, it is not enough that the values to be compared be much bigger than the noise. The values must also encompass a *range* which is much bigger than the noise. For spectral comparisons, this means that the data should contain slopes of peaks. For comparisons of slices, most of the slice, including the center, should be included.

First, the effects of air and cure speed on the imidization process will be quantified using PA spectra (Figures 11 to 13) from the centers of the dither cycles. Match factors calculated over three spectral ranges are given in Table V. Please refer to Figures 11, 12 and 13 to see which spectral details were included in the matches.

The matches in Table V demonstrate that PI 2525 shows a discernable effect from curing in air and no effect from cure speed. The narrower spectral ranges show the effect of curing in air more clearly. PI 2545 shows a similar sensitivity to curing in air but, under the conditions used here, is not sensitive to cure speed. PI 2611 shows a little variability in cure, but there is no correlation with air or cure speed. The different polyimides can easily be distinguished from one another.

The feasibility of depth-profiling will be assessed using the spectra from the bilayer specimens. If effects such as bi-layers can not be seen clearly, then resolving smaller effects such as small differences in degree of cure and differing orientations in thin layers will certainly not be practicable. To monitor the polyimide layers over their thickness, matches were calculated between slices through the time-delayed PA spectra.

Slices were taken at the following wavelengths (see Figure 9):

1504 cm^{-1} to set the relative scale of the each spectrum

1734 cm^{-1}, an intense absorbance which serves to monitor the composition of the surface of the specimen

1674 cm^{-1}, a medium-intense absorbance where the spectra of the pure materials show that the absorptivities of the top and bottom layers in the bilayer materials differ considerably

1617 cm^{-1}, similar to 1674 cm^{-1} but a less-absorbing and less-distinguishing region of the spectra.

These slices from specimens 19 (PI2525), 22 (PI 2545), 45, 46 and 47 (bi-layers) are plotted in Figure 16. Inter-slice matches were calculated. Poor matches were obtained initially, which showed that the phases of the slices must be well synchronized before the absorbances in the slices can be meaningfully matched. The spectrometer measured the time-delayed spectra in fixed intervals of 10 degrees in phase, and the slices are generated with the highest absorbance in the spectrum defining phase angle zero. There is of course no guarantee that zero phase falls in a measured position in the dither cycle. A crude correction for poor definition of the zero phase angle was implemented by shifting the slices along the abscissa until the peak scaling peaks at 1502 cm^{-1} were seen to overlap well. New matches were calculated, interpolating where necessary to obtain the appropriate value for a slice. The first column of matches in Table VI used all spectra in the slices. In the three remaining columns, only those components with maximum absorption >0.3 were used, which served to clip off regions at the ends of peaks where gross mismatches occurred because the peaks had different phase angles (Figure 16).

The first line of Table VI shows that 22 and 34 agree well for intense absorbances but differ when compared to "medium depth". 22 is significantly thinner than 34. The underlying glass contributes to the spectrum even when the polyimide is probed to "medium depth".

The comparisons between the bilayers and the shallowest depth ("2 highest" column in Table VI) confirm, as was already clear from the PA spectra from the center of the dither cycle (Figure 9), that PI 2545 is the top layer of the bilayer specimens, since the matches of the bilayers with 22 and 34 are higher than those with 19. 47 matches less well with 22 and 34 than do 45 and 46, probably because it has a thinner overlayer. 47 has a significantly smaller total thickness than do 45 and 46, and probably also has a thinner underlayer, which makes it match more poorly with 19 than do 45 and 46. Because 45 matches the top layer better than does 46, and also matches the bottom layer better than does 46, 45 appears to be have somewhat thicker top and bottom layers than 46 does. Since the bottom layers contribute appreciably to the spectra of the bilayer materials, the top layer thicknesses are clearly much less than the thermal depth.

A problem appears with the comparison of 45, 46 and 47 with 22 and 34 at medium depth. Because 47 is thin, there is not enough absorption to make the third slice (1616 cm^{-1} in Figure 14) as big as the corresponding slices in 19, 45 and 46. Hence 47 looks more like 22 and 34. This effect is repeated in the fourth slice, where the radiation probed the most deeply. However, the match with 19 for the greatest depth of penetration suggests that 47 is least like 19, which is probably true because 47 is believed to have the thinnest underlayer. This is also consistent with 45/47 being more different than 45/46 and 47/46, since 45 is the thickest bilayer specimen.

Thus, although one can rationalize the calculated match factors when the experimental details are already known, the experimental details have been too compressed in calculating the match factors to allow easy interpretation from the match factors alone. Better interpretations are possible when the details of the slices are visible. For example, the slice for 1734 cm^{-1} visually places PI 2525 in a different class from the other polyimide specimens. The slice for 1679 cm^{-1} places the bilayers between the pure materials and suggests from the phase lag of all but the PI 2525 specimens that the bilayer specimens and the PI 2545 specimens are closely related. 45 is clearly more like 19 than is either 46 or 47.

The results of the match comparisons reflect the dominating contribution of the specimen thicknesses. The bilayer with the thickest top (45) is most like the top layer version (22 and 34) of PI 2545. The same bilayer has the thickest underlayer and is most like the bottom layer.

The correlation calculation condenses all the spectral comparisons into one number. An exploration was made to see how to best add more components to the index. From Figure 16, the first contender for an expanded index is the height of the slice (the absorption at the center of the dither cycle) and the second is the phase (position of the maximum along the abscissa). The set of time-delayed spectra then are only important in establishing the values in the center slice, which, as has been described, may not have fallen exactly on a thumb wheel position on the lock-in amplifier. To include some information from the complete slice, asymmetry of the peak

was considered. The origin of the abscissa was placed at the peak maximum of each peak in the slices and the peak shapes were fitted by a second degree polynomial. The results are given in Table VII. The fact that the linear component was effectively zero shows that there was no asymmetry in the peak shapes. Therefore, the peak shapes are parabolic. There was of course then very good correlation between the coefficient of the squared term and the peak height. Examination of Table VII shows that the relative phase angle correlates with increased depth of penetration, phase advance denoting less penetration and smaller absorbance and phase retardation denoting more penetration and less absorbance. This information is already present in the heights of the peaks. Because the peaks are so regular in shape, this is essentially a repeat of the slice analysis detailed earlier.

To unravel the relationships between the single layer specimens 19, 22 and 34 and the double layer specimens 45, 46 and 47, it is probably best to follow changes over narrow ranges of wavenumbers. Table VIII shows the discrimination obtained if the surface spectra (with time delay of zero) of double-layer and single layer specimens are compared. For the spectral range 600-2800 cm^{-1} there is no clear matching of the dual layer to the polyimide known to be in the top layer of the composite (top half of Table VIII). Many of the details in the spectral range are very similar in all spectra of these polyimides and these similarities dominate the match factors, which are therefore unable to distinguish between the various spectra. Visual inspection of the spectra suggested that noticeable differences occurred in the region 600-1000 cm^{-1}. This is confirmed quantitatively by the match indices given in the second half of Table VIII, where the match factors are seen to be more discriminating and it is unequivocally clear that PI 2545 is the top polyimide and at least strongly indicated that PI 2525 is the bottom polyimide, with 47 having the thinnest top layer, 46 having a somewhat thicker top layer (poorer match with PI 2525, better match with PI 2545) and 45 having the thickest top layer (worst match with PI 2525 and the best match with PI 2545).

Refractive Indices of Films
Coburn and Pottiger (16) have demonstrated the utility of birefringence in assessing the anisotropy of a polyimide layer. The birefringences given in Table I show there is very little anisotropy in the PI 2525 layers. There is more anisotropy in the PI 2545 layers and a noticeable variation of anisotropy with film thickness as noted by Coburn and Pottiger. The PI 2611 layers all have approximately the same amount of birefringence, which is much greater than those of the other polyimides. There is no obvious difference between fast and slow cures. The specimens were removed from the substrates by soaking them in water before the refractive index measurements were made. This undoubtedly plasticized the polyimide films and probably removed 1) all of the anisotropy induced by stress between the substrate and the film and 2) some of the anisotropy in the film itself. Secondly, all specimens in this study were necessarily cooled from 350°C to room temperature over 16 hours because of the large mass of the oven used. This may have allowed some annealing to occur which reduced differences arising from different cure rates. Thirdly, the cure rates recommended by the supplier may have already been optimized to reduce dependency of cure and orientation on heating rate.

X-Ray Data

The polyimide/glass plate specimens were mounted in a wide-angle X-ray diffractometer equipped with a two-theta, two-circle goniometer. Diffraction patterns were necessarily taken in reflection mode over a 2θ range of $10°$ to $30°$ using Cu-Kα radiation and narrow incident and receiving collimation slits. Coburn and Pottiger show that order is indicated in reflection mode by the appearance of a shoulder or a peak, depending on the final temperature in the cure cycle, at about $25°$ 2θ and that order in these polyimide films is much more apparent in transmission diffraction patterns.

The reflection diffraction patterns were corrected for background by subtracting the diffraction pattern obtained from an empty glass plate. Comparisons of diffraction data for slow and fast curing are shown in Figures 17 to 19. In each case, the upper curve represents the slow cure. There is no marked difference in scattering for fast and slow cures. A shoulder at $25°$ 2θ, consistent with Figure 5 of Coburn and Pottiger, may indicate slightly more order in the slowly-cured specimen of PI 2611 on the glass, but this is not evident in the birefringence measurements on the free films and is not indicated by the PAS measurements.

In the case of PI 2525, there is essentially no additional X-ray scattering from the slowly-cured specimen if the ends of the scattering envelopes are put at the same height. None of the techniques suggests that there is any difference in order in these specimens.

In the case of PI 2545, the X-ray scattering shows marginally more intensity for the slowly-cured specimen but the evidence for more order in the slowly cooled specimen is not definitive. The specimens differ too much in thickness for the refractive index data to be able to be informative about more order in the slowly-cured PI 2545 specimen. The PAS technique indicates that there is not more order in the slowly-cured PI 2545 specimens. The PAS technique is considerably quicker than the X-ray technique in comparing these specimens, although in the PAS technique only differences are found, not whether or not there is more order *per se*. The PAS technique is much slower than the refractive index technique.

Conclusions

PAS spectra can be used to compare layer specimens over their thermal depths, with the depth probed being constant across the spectrum. The dither frequency of 400 Hz used here established a thermal depth of about 22 micrometers for a polyimide film. (Increasing the dither frequency to 800 Hz decreases the thermal depth to 15 μm.) Both time-sliced and non-time sliced step scan spectra can be used but there seems to be no advantage in using time-sliced spectra over non-time slice since most if not all the information is given by the heights of the spectral absorptions. The information in a series of time-sliced spectra can be condensed into a simple peak-like data set by slicing through the time-sliced spectra. Non-time sliced spectra can be compared using short spectral ranges. Sets of such data have been compared numerically. The numerical match index, actually a correlation factor, indicates the extent to which the two specimens differ over their "thermal depths". Different polyimides can easily be distinguished from one another and the effect of small differences in curing in nitrogen or air and of

differences in layer thickness can be discerned.

The spectra of thermally-thin two-layer specimens taken at zero delay discriminate successfully between surface layers of different thicknesses. Discerning the presence of a different under-layer when the over-layer is very similar to the under-layer is a difficult task, but the procedure is able to differentiate between two such layers.

Acknowledgements

References

1. F. Garbassi and E. Occhiello, Analytica Chim. Acta, **197** 1 (1987).

2. F.M. Mirabella, Jr., J. Polym. Sci., Phys. Ed. **23**, 861, (1985).

3. A.G. Bell, Am. J. Sci. **20**, 305 (1880); Philos. Mag. **11**, 510 (1881).

4. A. Rosencwaig, Opt. Commun., **7**, 305 1973; Science **181**, 657 (1973).

5. A. Rosencwaig and A. Gersho, J. Appl. Phys. **47**, 64 (1976).

6. H.S. Bennett and R.A. Foreman, Appl. Opt. **15**, 347 (1976); Appl. Opt. **15**, 2405 (1976); J. Appl. Phys. **48**, 1432 (1977).

7. F.A. McDonald and G.C. Whetsel, Jr. J. Appl. Phys. **49**, 2313 (1978).

8. F.A. McDonald, J. Opt. Soc. Am. **70**, 555 (1980).

9. M.J. Smith, C.J. Manning, R.A. Palmer and J.L Chao, Appl. Spectrosc. **42**, 546, (1988).

10. L. Bertrand, Appl. Spectrosc. **42**, 134 (1988) and references therein.

11. J.C. Roark, R.A. Palmer and J.S. Hutchison, Chem. Phys. Lett. **60**, 112 (1978).

12. Y.C. Teng and B.S.H. Boyce, Optic. Soc. America **70**, 557 (1980 [15])).

13. R.M. Dittmar, J.L. Chao and R.A. Palmer, Appl. Spectrosc., **45**, 1104 (1991).

14. Commercial materials are identified to specify the procedures and specimens used. Such mention is not to be construed as endorsement of these materials.

15. C.J. Manning, R.M. Dittmar and R.A. Palmer, Infrared Phys. **33**, 53 (1992) and references therein.

16. J.C. Coburn and M.T. Pottiger, in "Advances in Polyimide Science and Technology", Proc. 4th Intl. Conf. Polyimides, C. Feger, M.M. Khojasteh and M.S. Htoo, eds., Technomic Publ., Lancaster, PA, (1992).

17. R.O. Carter, III, M.C. Paputa Peck, M.A. Samus and P.C. Killgoar, J. Appl. Spectrosc. **43**, 1350 (1989).

18. C.A. Pryde, J. Polym. Sci. A Chem., **31**, 1045, (1993).

19. R.W. Synder, B. Thomson, B. Bartges, D. Czerniawski and P.C. Painter, Macromolecules, **22**, 4166 (1989).

20. K.A. Brownlee, "Statistical Theory and Methodology in Science and Engineering", Wiley, p56 1960.

21. L. Huber, in "Applications of Diode Array Detection in High Performance Liquid Chromatography", Hewlett-Packard Publication 12-5953-2330 (1989).

Table I Details of PI Specimens Cured on Small Glass Plates

PI	No.	RPM	Thickness micrometer (rim)	Thickness ew (TE) (center)	RI (TE)	Thickness ew (TM) (center)	RI (TM)	birefring.
Slow ramp in N$_2$								
2525	19	3000	20.9	11.9 (2)	1.6540	12.59 (7)	1.6400	0.0140
2525	20	2500	11.0	9.7 (5)	1.6539	9.79 (8)	1.6373	0.0166
2545	21	2000	10.0	5.01 (6)	1.6812	5.7 (4)	1.5970	0.0842
2545	22	1000	16.2	12.11 (7)	1.6775	12.3 (1)	1.6074	0.0701
2611	23	3000	13.3	10.1 (1)	1.7858	10.8 (1)	1.5860	0.1998
2611	24	2500	7.8	9.42 (4)	1.7836	9.68 (9)	1.5860	0.1976
slow ramp in air								
2525	25	2700	14.7	13.04 (3)	1.6541	13.15 (3)	1.6424	0.0117
2525	26	2700	17.5	12.63 (9)	1.6537	12.4 (7)	1.6405	0.0132
2545	27	1200	8.0	9.07 (6)	1.6783	9.86 (2)	1.6078	0.0705
2545	28	1200	---	11.10 (9)	1.6749	11.64 (7)	1.6066	0.0683
2611	29	3000	11.5	lost				
2611	30	3000	29.9	11.13 (8)	1.7786	11.1 (2)	1.5943	0.1843
fast ramp in N$_2$								
2525	31	2700	15.0	lost				
2525	32	3500	15.0	9.6 (1)	1.6536	9.6 (2)	1.6417	0.0119
2545	33	1000	34.0	11.62 (8)	1.6747	11.4 (2)	1.6136	0.0611
2545	34	800	36.6	22.5 (3)	1.6763	24.5 (3)	1.6258	0.0505
2611	35	3000	23.5	8.7 (1)	1.7871	9.13 (7)	1.5895	0.1976
2611	36	3000	18.7	7.94 (7)	1.7884	8.60 (6)	1.5892	0.1992
Slow ramp in N$_2$ (repeat of 19)								
2525	39	2500	19.7	22.1 (2)	1.6542			
2525	39	2500	19.7	11.96 (9)	1.6536	11.98 (8)	1.6359	0.0177
mix	45							
mix	46							
mix	47							

PI = Polyimide type; No. = specimen number; RPM = revolutions per minute of spin-caster, most specimens spun for 30 s; rim thickness measured with micrometer; center thickness measured with optical waveguide technique; ew = evanescent wave; TE = transverse electric field configuration; TM = transverse magnetic field configuration; RI= refractive index; birefring. = birefringence. The PI layers typically had a raised rim at the edge of the glass plate, with considerable non-uniformity in thickness as reflected in the differences between the rim and the center thicknesses.

Table II Cure Schedules of Polyamic Acid Solutions

Slow cure in N_2:

1) N_2 flowed through oven until O_2 content <0.3%
2) Heat at 2 °C per min to 135 °C
3) Hold at 135 °C for 30 min
4) Heat at 2 °C per min to 200 °C
5) Hold at 200 °C for 30 min
6) Heat at 2 °C per minute to 350 °C
7) Hold at 350 °C for 60 min
8) Cool slowly over 16 h

Slow cure in air: no N_2 flowed through oven.
Temperature program as for N_2.

Fast Cure in N_2:

1) N_2 flowed through oven until O_2 content <0.3%
2) Heat at 20 °C to 40 °C per min to 350 °C
3) Hold at 350 °C for 60 min
4) Cool slowly over 16 h

Table III Wavenumber set used to generate initial set of slices
698, 725, 737, 825, 858, 875, 931, 978, 1554, 1852, 1874, 1894, 3474 cm^{-1}

Table IV Thicknesses in the PI bilayers

sample ID	top (μm)	bottom (μm)
45	7.5	52
46	3.1	12
47	4.4	6.6

(Thicknesses imprecisely estimated from micrometer readings)

Table V Matches calculated between center-of-dither-cycle spectra for PI 2525, PI 2545 and PI 2611 cured at 2°C/min (slow) and 20°C/min (fast) in N_2 and 2°C/min in air. Perfect match = 1.000

PI 2525	1300-1800 cm⁻¹	1640-1800 cm⁻¹	1750-1800 cm⁻¹
slow (19) / slow (20)	0.999 1.000	1.000	
slow (19) / slow (39)	0.999 0.999	1.000	
slow (20) / slow (39)	0.998 0.998	0.999	
slow (19) / fast (31)	0.999	0.999	0.995
slow (20) / fast (31)	0.999	0.999	0.999
slow (39) / fast (31)	0.998	0.998	0.997
N_2 (19) / air (26)	0.992	0.987	0.985
N_2 (20) / air (26)	0.992	0.986	0.982
N_2 (31) / air (26)	0.993	0.987	0.981
N_2 (39) / air (26)	0.992	0.986	0.985

PI 2545	1300-1800 cm⁻¹	1640-1800 cm⁻¹	1750-1800 cm⁻¹
slow (22) / fast (34)	0.997	0.999	0.998
N_2:slow (22) / air (27)	0.990	0.980	0.836
N_2:fast (34) / air (27)	0.985 0.976	0.841	

PI 2611	1300-1800 cm⁻¹	1640-1800 cm⁻¹	1750-1800 cm⁻¹
slow (23) / slow (24)	0.997 0.996	0.998	
fast (35) / fast(36)	0.996	0.999	0.999
slow (23) / fast (35)	0.999	0.998	0.998
slow (23) / fast (36)	0.998	0.996	0.995
slow (24) / fast (35)	0.998	0.999	1.000
slow (24) / fast (36)	0.998	0.998	0.999
N_2:slow (23) / air (30)	0.999	0.999	1.000
N_2 slow (24) / air (30)	0.996	0.993	0.998
N_2 fast (35) / air (30)	0.999 0.997	0.998	
N_2 fast (36) / air (30)	0.998 0.996	0.998	

Different polyimides
slow

	1300-1800 cm⁻¹	1640-1800 cm⁻¹	1750-1800 cm⁻¹
PI 2525(19) / PI 2545(22)	0.834	0.740	0.342

fast
PI 2525(31) / PI 2545(34) 0.841   0.705   0.407

slow
PI 2525(19) / PI 2611(24) 0.655   0.583   0.270
fast
PI 2525(31) / PI 2611(36) 0.639   0.574   0.295

slow
PI 2545(22) / PI 2611(24) 0.740   0.906   0.749
fast
PI 2545(34) / PI 2611(36) 0.736   0.915   0.708

Table VI Match comparisons of the bilayers with the pure materials

	All 4 slices All absorbances	All 4 slices Absorbances > 0.3	3 highest	2 highest
		Depth probed:		
		deepest	medium	shallow
PI 2545 (22) / PI 2545 (34)	0.986	0.988	0.987	0.995
PI 2525 (19) / PI 2545 (22)	0.891	0.816	0.779	0.980
PI 2525 (19) / PI 2545 (34)	0.894	0.861	0.829	0.978
PI 2545 (22) / Bilayer (45)	0.957	0.934	0.918	0.997
PI 2545 (22) / Bilayer (46)	0.962	0.942	0.928	0.992
PI 2545 (22) / Bilayer (47)	0.974	0.959	0.948	0.983
PI 2545 (34) / Bilayer (45)	0.975	0.964	0.953	0.996
PI 2545 (34) / Bilayer (46)	0.976	0.968	0.959	0.993
PI 2545 (34) / Bilayer (47)	0.981	0.976	0.970	0.986
PI 2525 (19) / Bilayer (45)	0.956	0.944	0.933	0.981
PI 2525 (19) / Bilayer (46)	0.953	0.936	0.919	0.977
PI 2525 (19) / Bilayer (47)	0.935	0.907	0.881	0.960
Bilayer (45) / Bilayer (46)	0.993	0.998	0.998	0.998
Bilayer (45) / Bilayer (47)	0.990	0.989	0.985	0.996
Bilayer (46) / Bilayer (47)	0.991	0.994	0.993	0.990

Table VII Fitting parameters for peaks in PA slices

specimen		19	22	34	45	46	47
peak 1							
phase (center)	10.81	9.31	10.29	9.94	10.64	9.98	
parabolic		-0.0073	-0.0070	-0.0070	-0.0136	-0.0141	-0.0130
linear		0.000	0.000	0.000	0.000	0.000	0.000
height		0.718	0.695	0.676	1.371	1.403	1.290
residual error		0.008	0.009	0.014	0.021	0.019	0.032
peak 2							
phase (center)		10.44	9.23	9.96	9.86	10.57	9.94
parabolic		-0.0111	-0.0097	-0.0092	-0.0192	-0.0201	-0.0183
linear		0.000	0.000	0.000	0.000	0.000	0.000
height		1.080	0.954	0.912	1.910	1.962	1.805
residual error		0.016	0.013	0.014	0.033	0.026	0.040
peak 3							
phase (center)		11.30	10.59	12.13	11.43	12.05	11.23
parabolic		-0.0067	-0.0038	-0.0039	-0.0104	-0.0107	-0.0090
linear		0.000	0.000	0.000	0.000	0.000	0.000
height		0.678	0.368	0.397	1.054	1.060	0.898
residual error		0.024	0.006	0.010	0.036	0.017	0.023
peak 4							
phase (center)		11.83	10.97	12.655	11.89	12.3711	11.63
parabolic		-0.0042	-0.0026	-0.0029	-0.0069	-0.0064	-0.0057
linear		0.000	0.000	0.000	0.000	0.000	0.000
height		0.409	0.253	0.291	0.672	0.674	0.558
residual error		0.004	0.007	0.009	0.014	0.024	0.010

Peaks in slices relative to first peak (standard) for each set

Peak 2	19	22	34	45	46	47
phase shift	-0.36	-0.08	-0.33	-0.08	-0.06	-0.04
parabolic ratio	1.52	1.39	1.31	1.41	1.43	1.41
height ratio	1.50	1.37	1.35	1.39	1.40	1.40
height/error*	67	73	65	57	75	45

Peak 3	19	22	34	45	46	47
phase shift	0.49	1.28	1.84	1.49	1.41	1.25
parabolic ratio	0.92	0.54	0.56	0.76	0.76	0.69
height ratio	0.94	0.53	0.59	0.77	0.76	0.67

| height/error* | 28 | 61 | 39 | 29 | 62 | 39 |

Peak 4

phase shift	1.02	1.66	2.37	1.95	1.74	1.65
parabolic ratio	0.58	0.37	0.41	0.51	0.45	0.44
height ratio	0.57	0.36	0.43	0.49	0.48	0.43
height/error*	102	36	32	48	28	55

* error = residual error

Table VIII **"Localized" Match Factors for Two-Layer Specimens v. Single layer Specimens using only the "Surface" Spectrum.**

Spectral Range 600-2800 cm^{-1} (no clear match)

polyimide	PI 2545	PI 2525	PI 2611
	top	bottom	neither
bilayer 45	.976	.979	.863
bilayer 46	.976	.981	.860
bilayer 47	.979	.978	.835

Spectral Range 600-1000 cm^{-1} (best match to top)

polyimide	PI 2545	PI 2525	PI 2611
	top	bottom	neither
bilayer 45	.899	.586	.475
bilayer 46	.885	.689	.478
bilayer 47	.845	.735	.442

"top" and "bottom" refer to the position of the polyimide in the two-layer film.
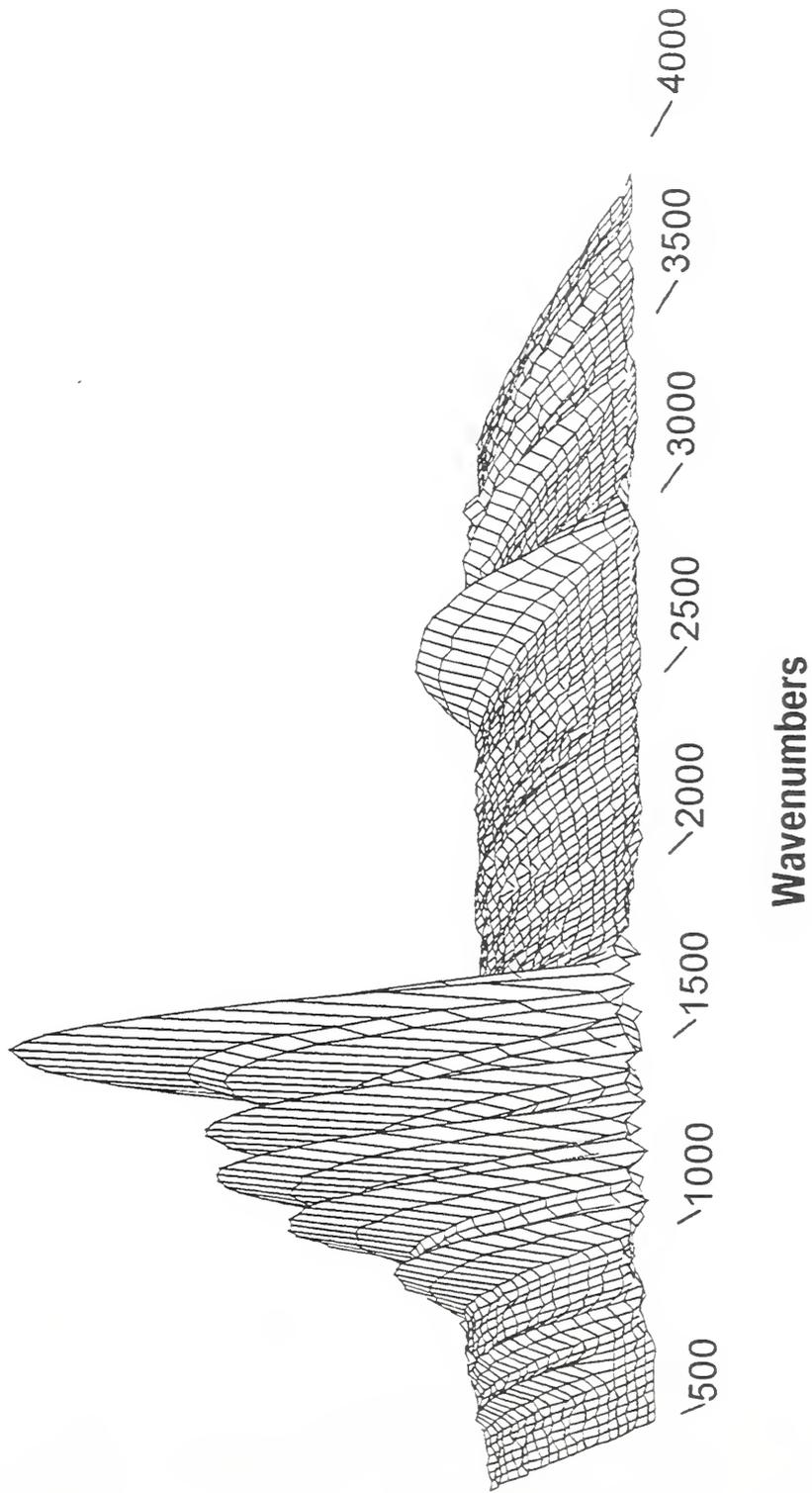
Figure 1: Time-delayed PAS spectra for PI 2525 on glass, showing changes in absorption (vertical axis) with mirror position in the dither cycle (axis perpendicular to the page).

Wavenumbers

500 1000 1500 2000 2500 3000 3500 4000
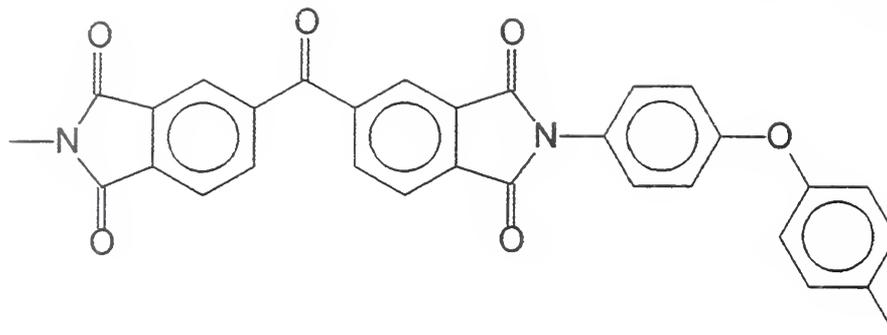
BTDA-ODA (Flexible)   [2525]
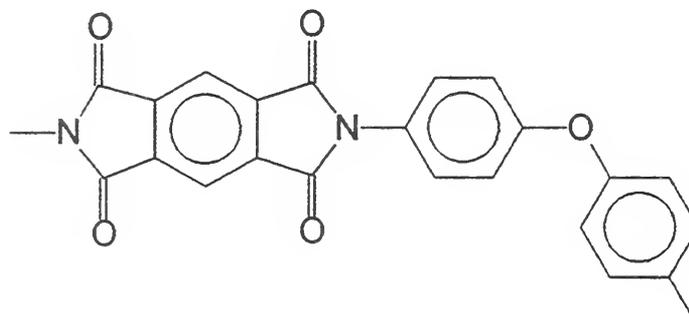
PMDA-ODA (SemiFlexible)   [2545]
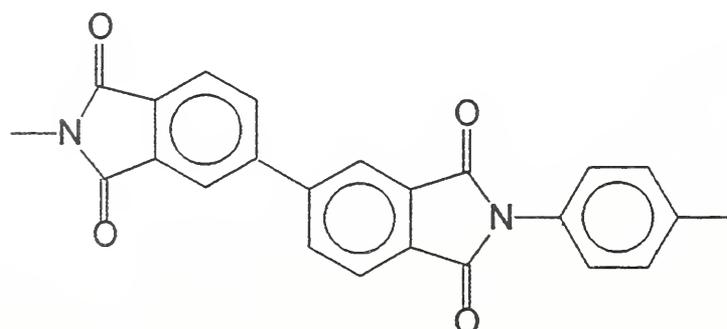
BPDA-PDA (Semi-Rigid)   [2611]

Figure 2: Idealized chemical formulae for the three polyimides.
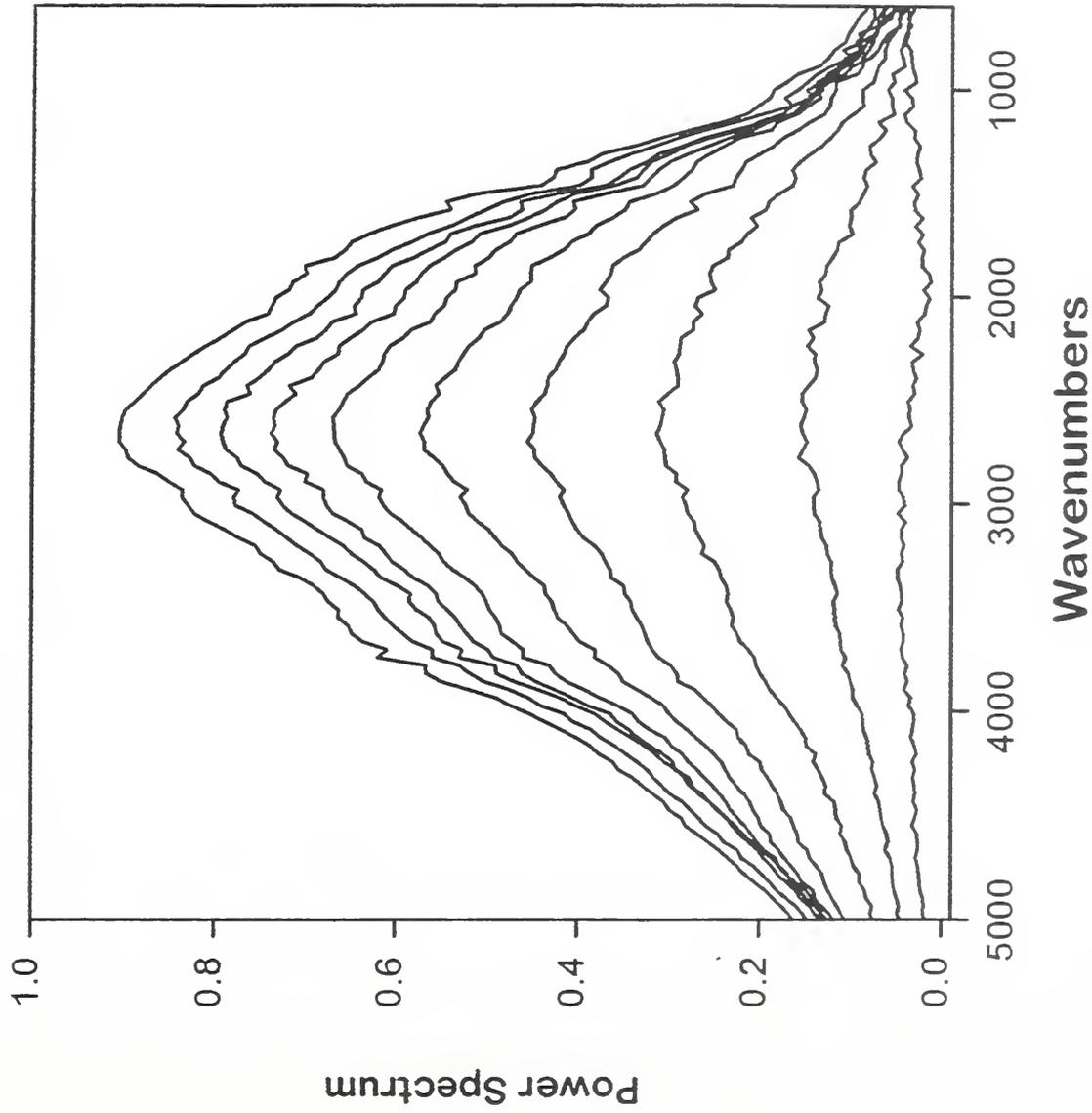
Figure 3: Variation of the PA spectral power distribution with mirror position in the dither cycle.
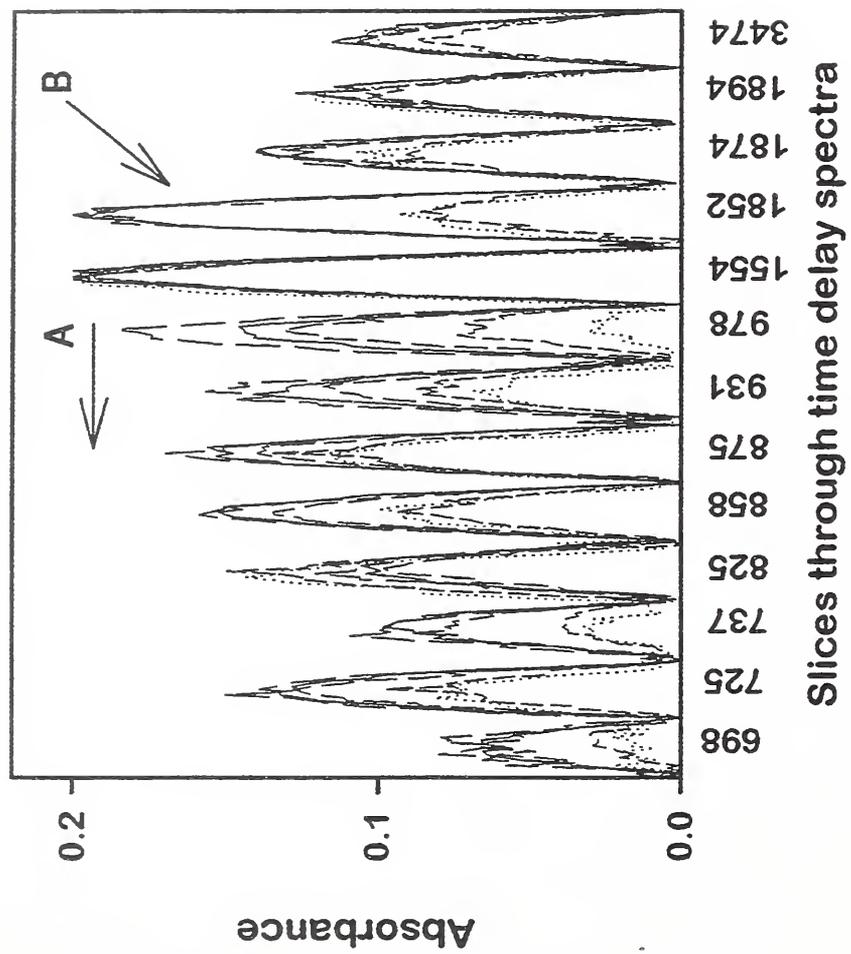
Figure 4: Slices through time-delayed PA spectra for PI 2525 and PI 2545 on glass.
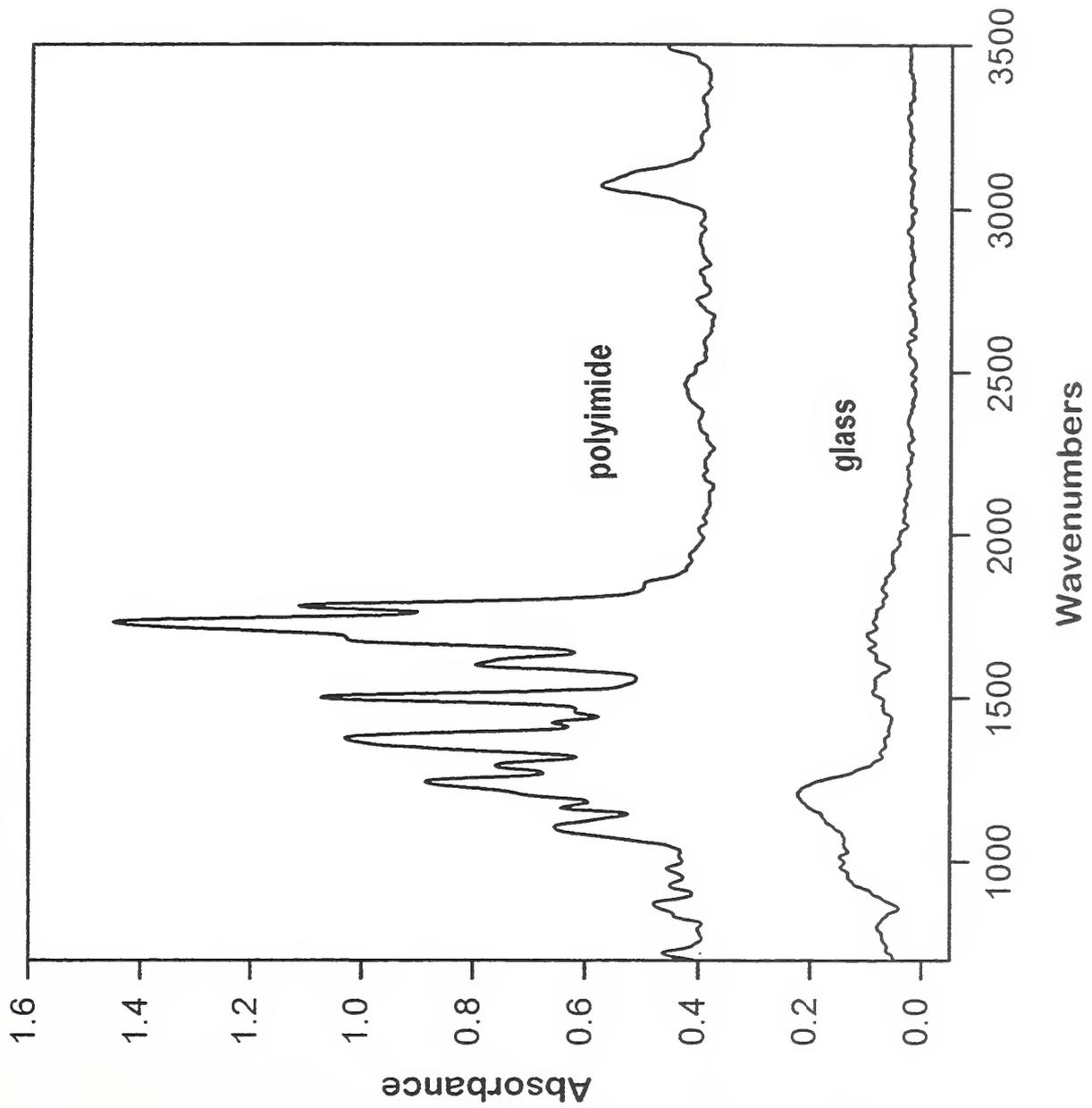
Figure 5: PA spectra from a polyimide and the glass substrate, both at the center of their dither cycles.
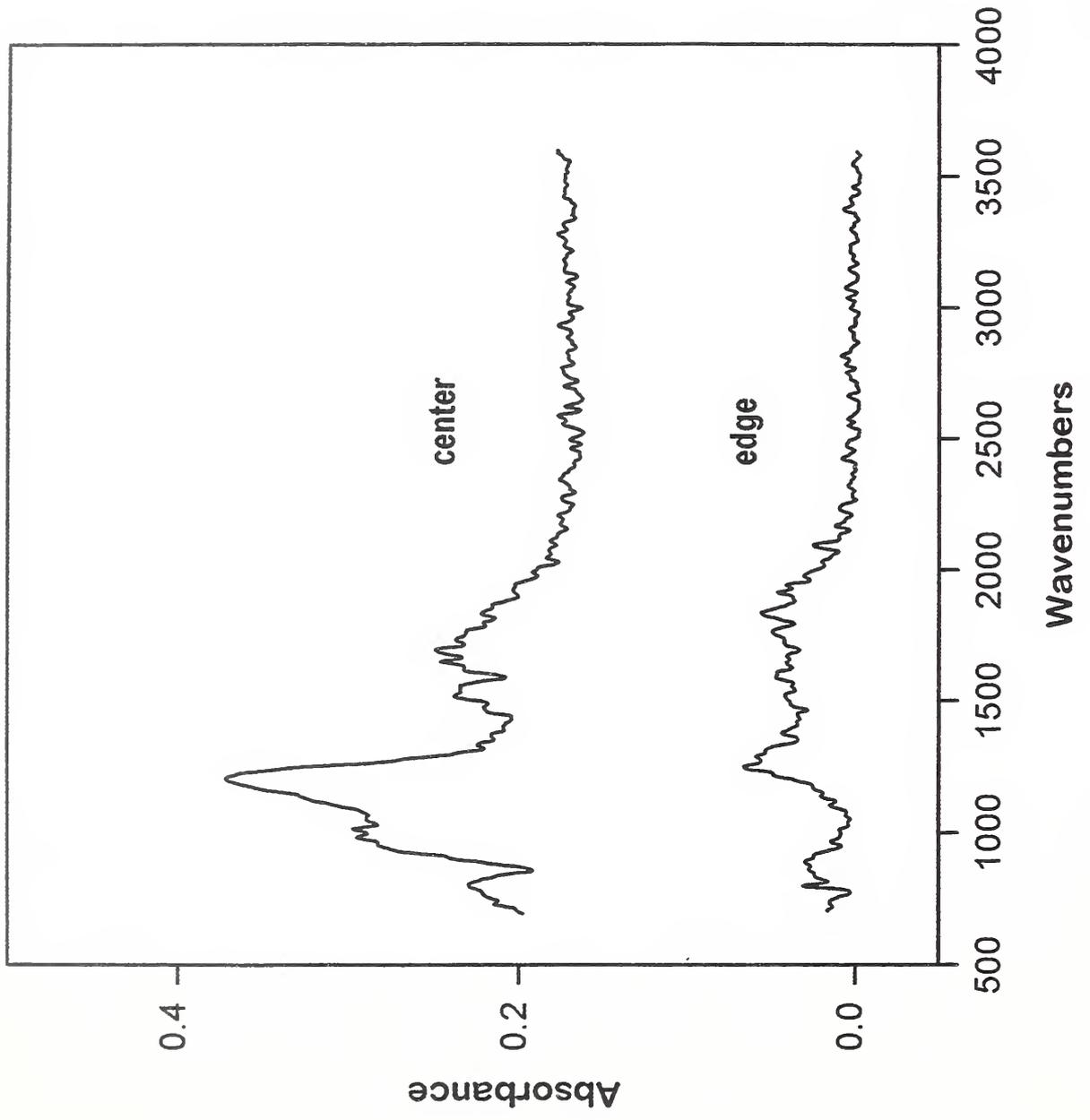
Figure 6: PA spectra of the glass substrate at the center and end of the dither cycle.
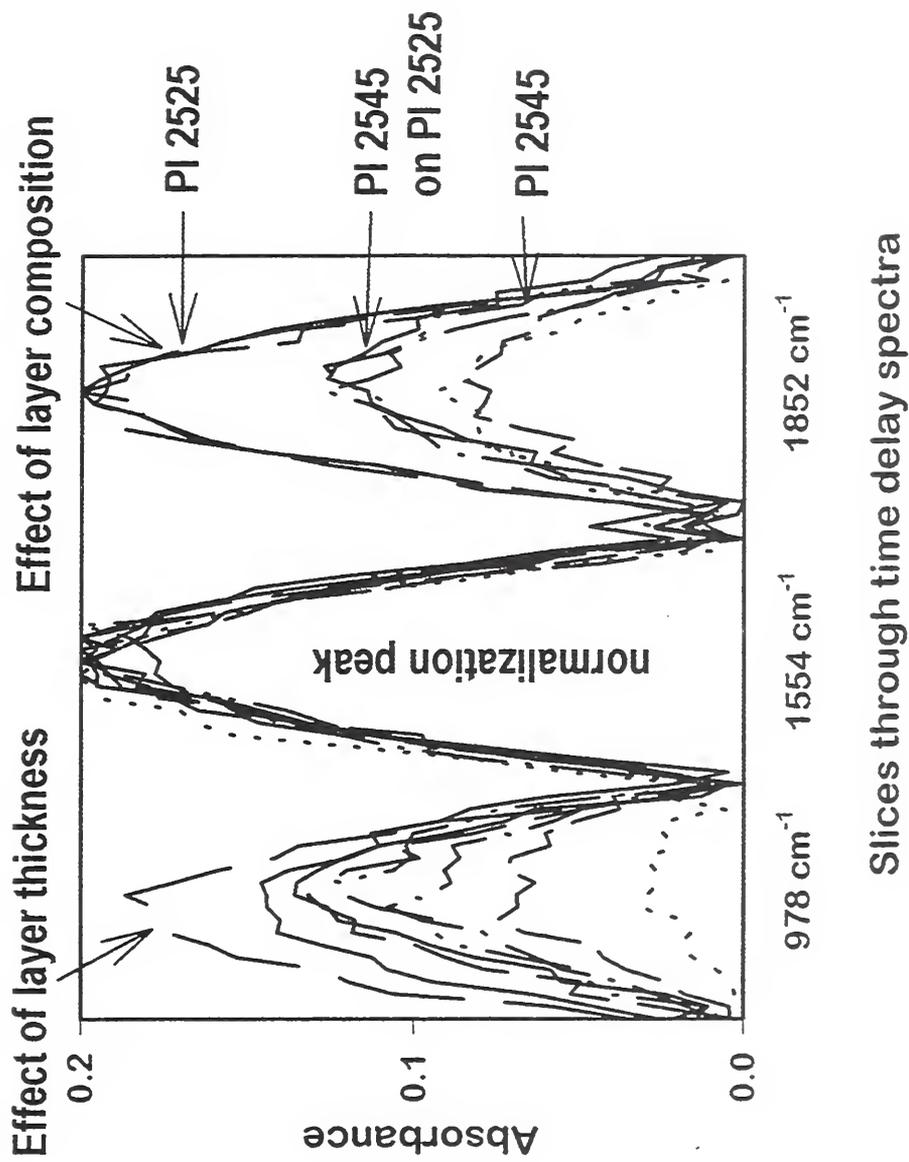
Figure 7: PAS slices for PI 2525, PI 2545, and bi-layer mixtures thereof.
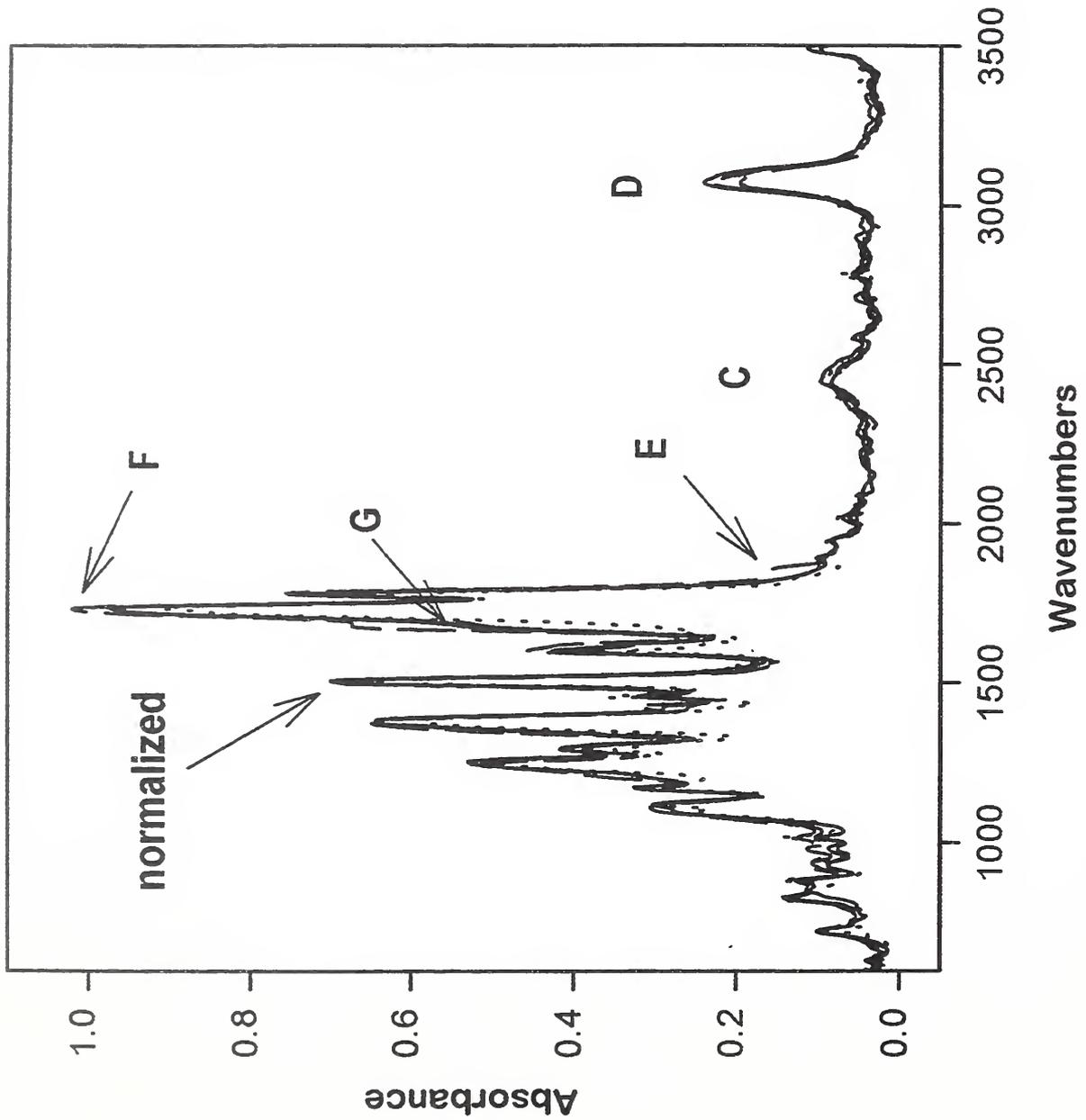
Figure 8: PA spectra of bi-layers of PI 2525 and PI 2545 and those of the pure materials, all on glass.
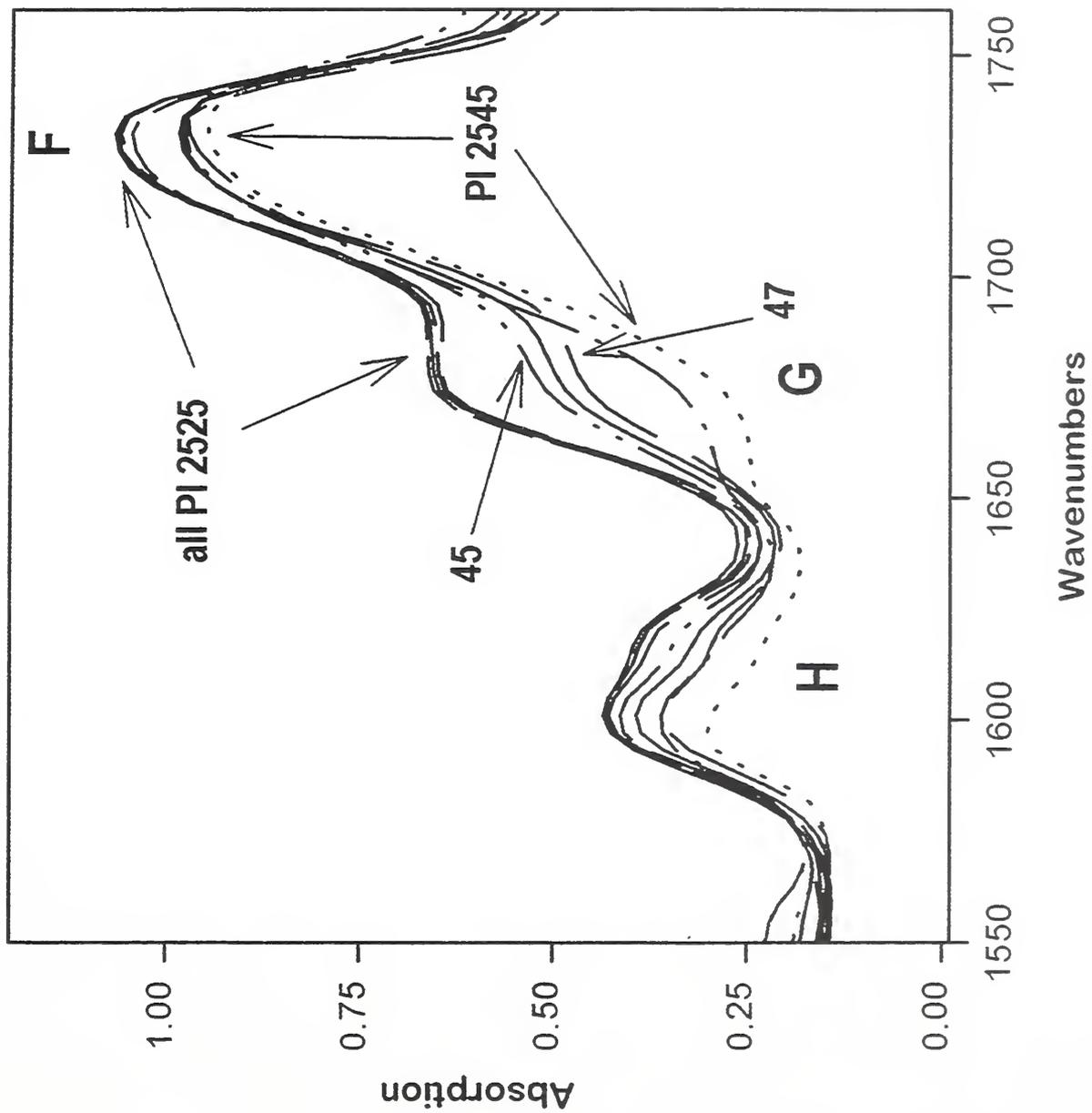
Figure 9: Comparison of PI bi-layers with the pure materials using the most intense part of the PAS spectrum.
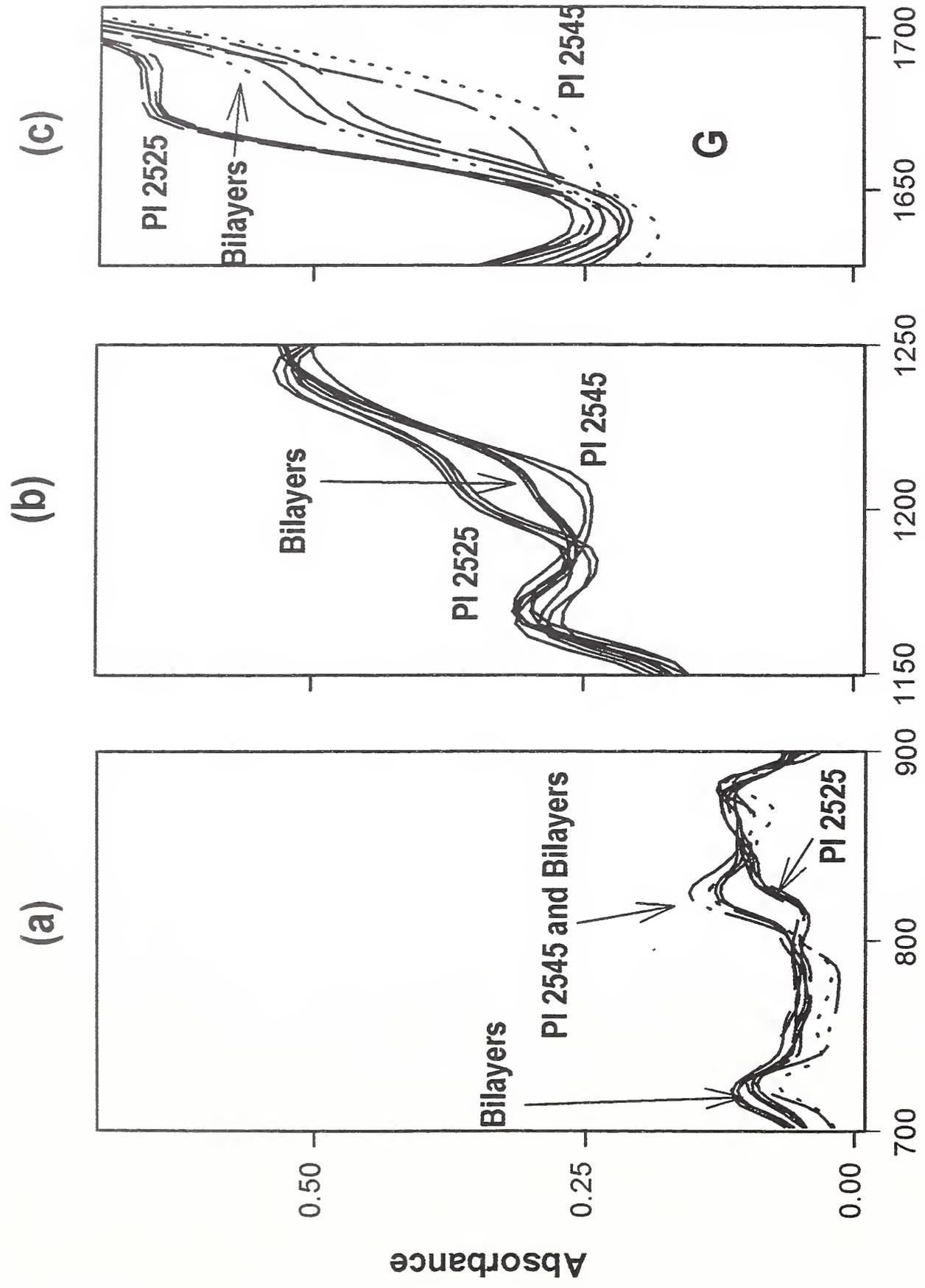
Figure 10: PAS differentiation of bi-layer structures from the pure materials.
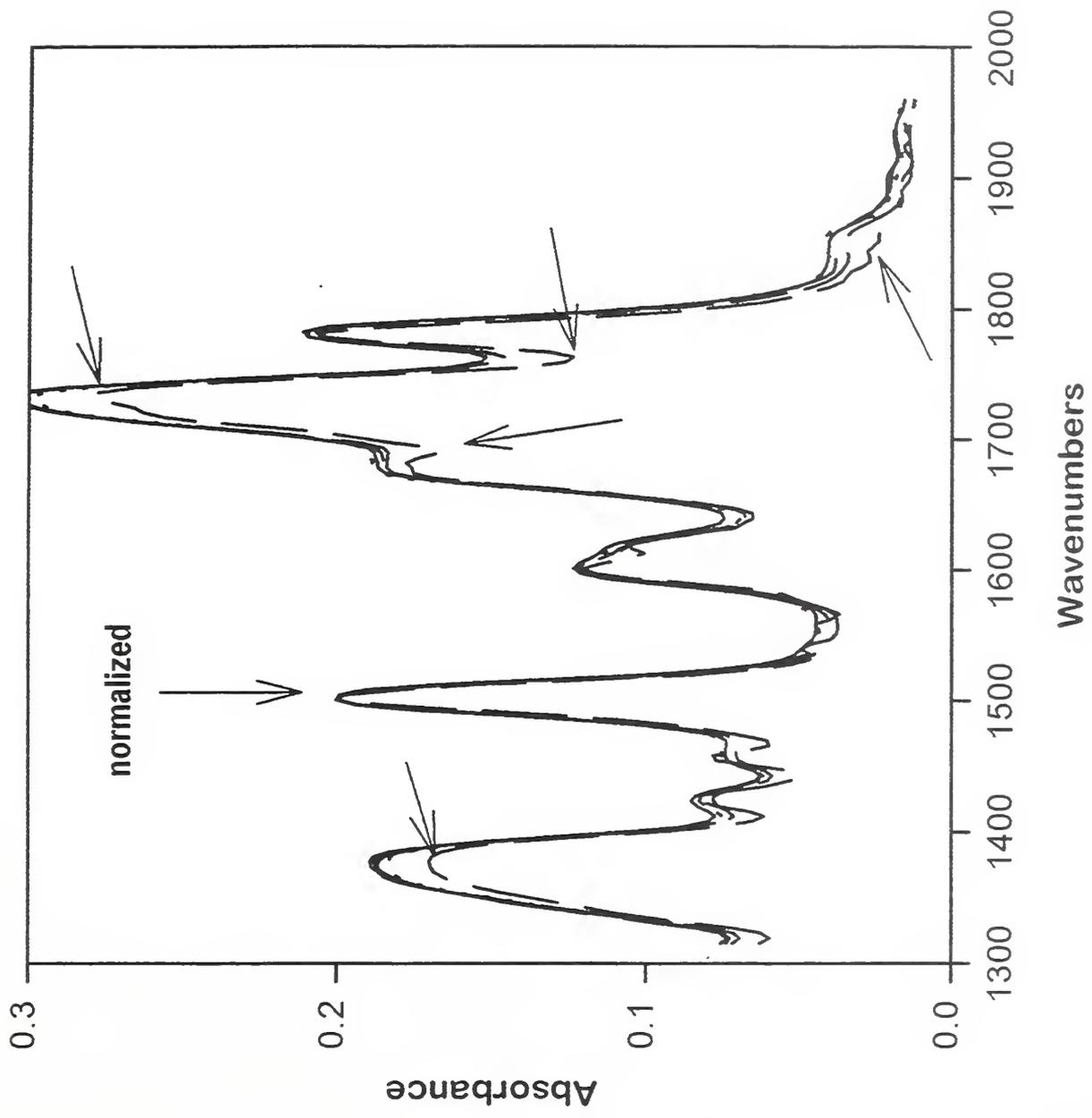
Figure 11: Effect of cure speed and air on PA spectra from PI 2525 (see text).
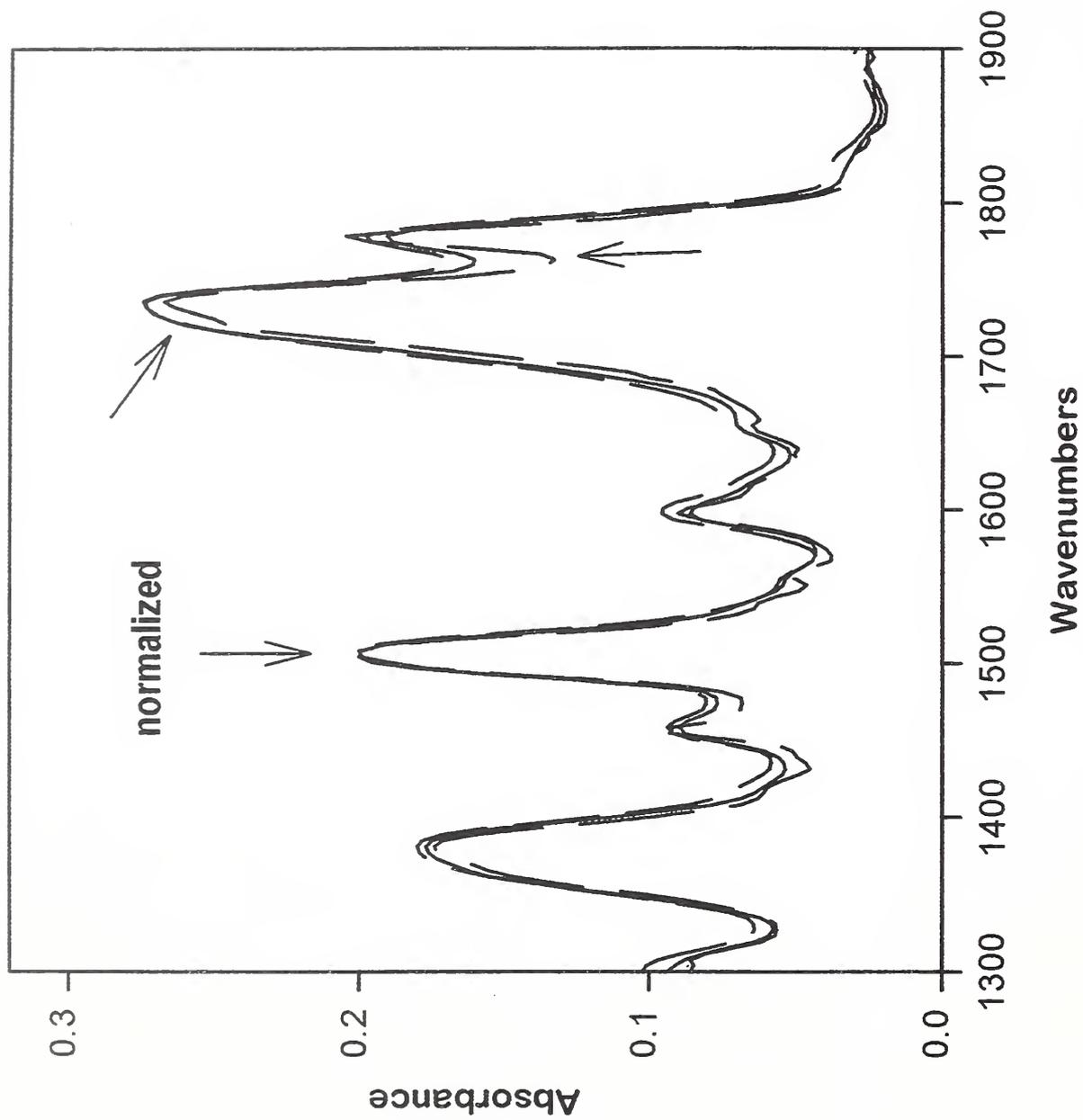
Figure 12:   Effect of air on the PA spectra of PI 2545 (see text).
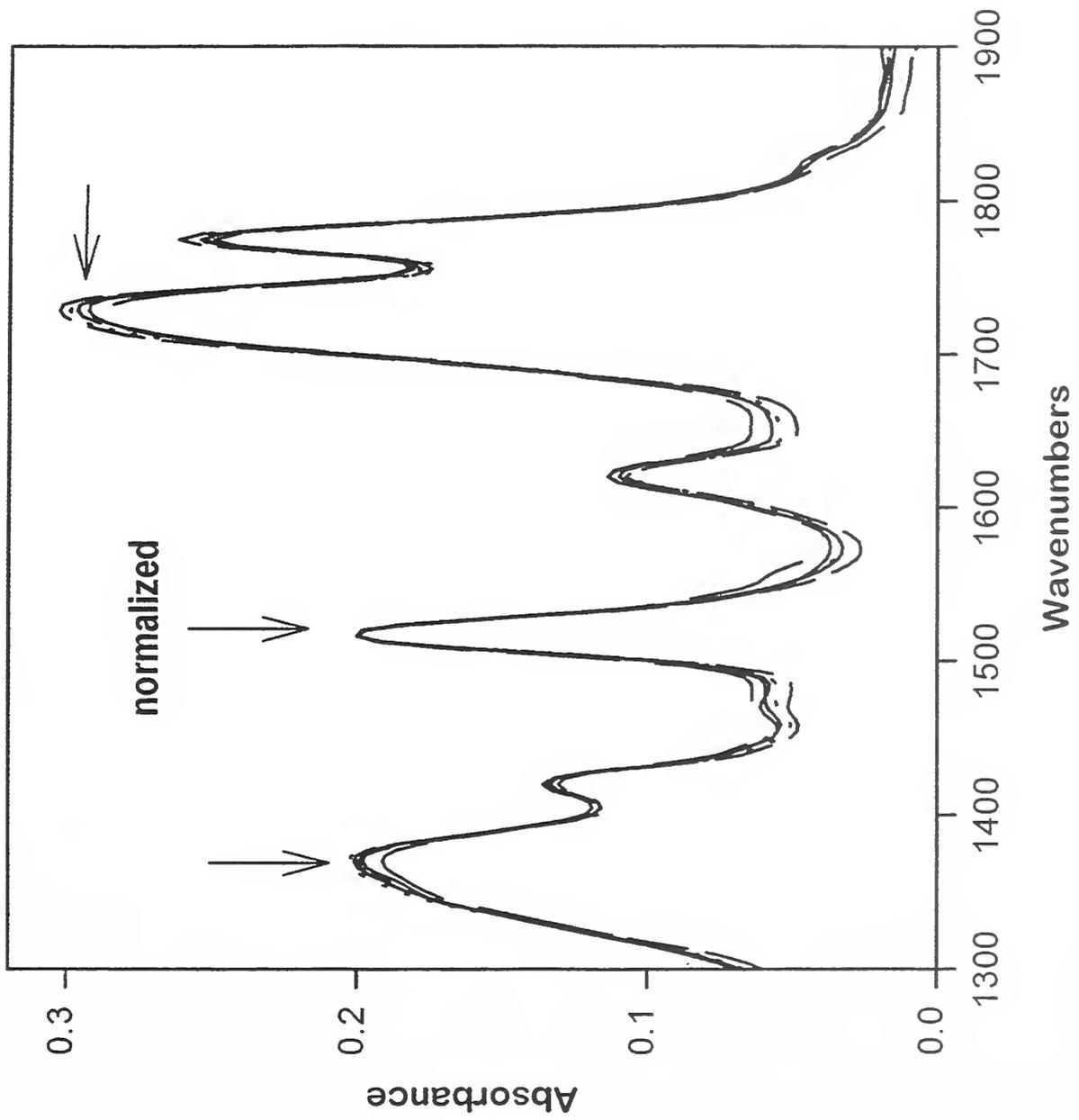
Figure 13: Effect of air on the PA spectra of PI 2611 (see text).
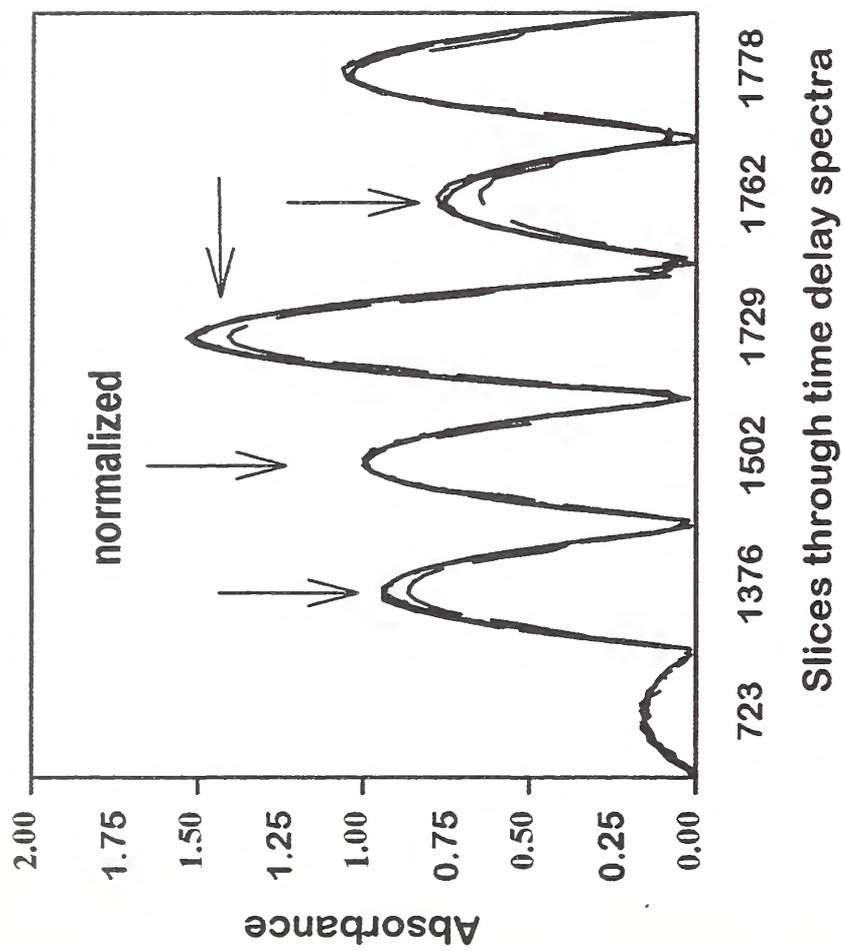
Figure 14: Slices through PA spectra for PI 2525 cured in N_2 at 2 °C/min and 20 °C/min and in air at 2 °C/min (see text).
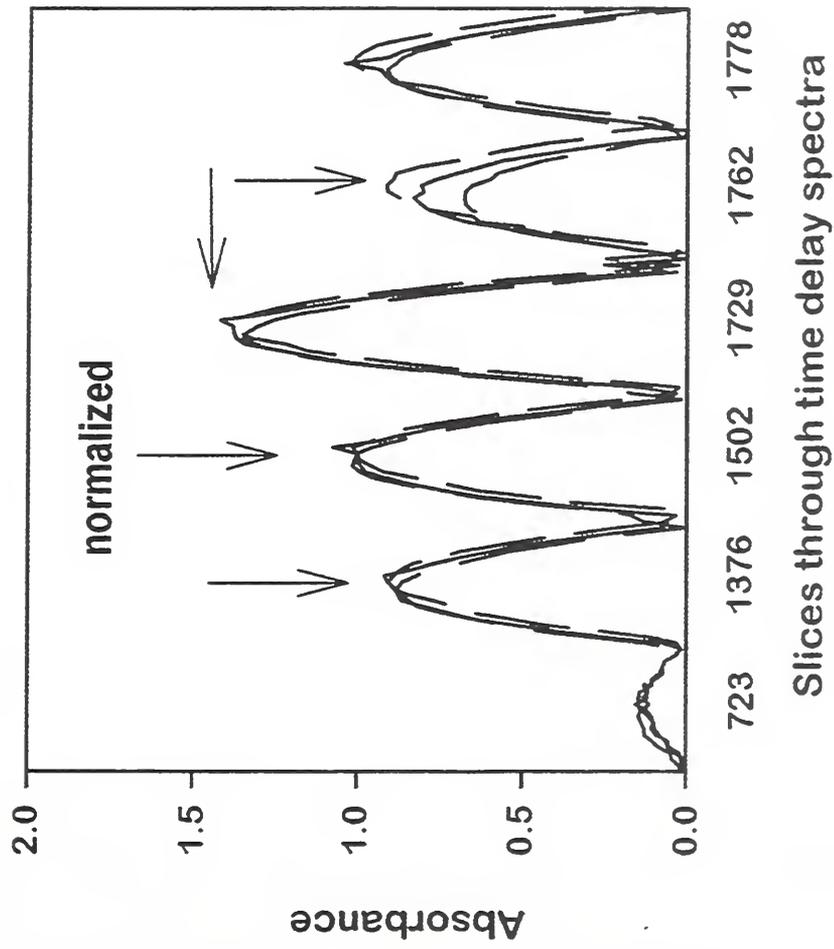
Figure 15: Slices through PA spectra for PI 2545 cured at 2 °C/min and 20 °C/min in N_2 and 2 °C/min in air (see text).
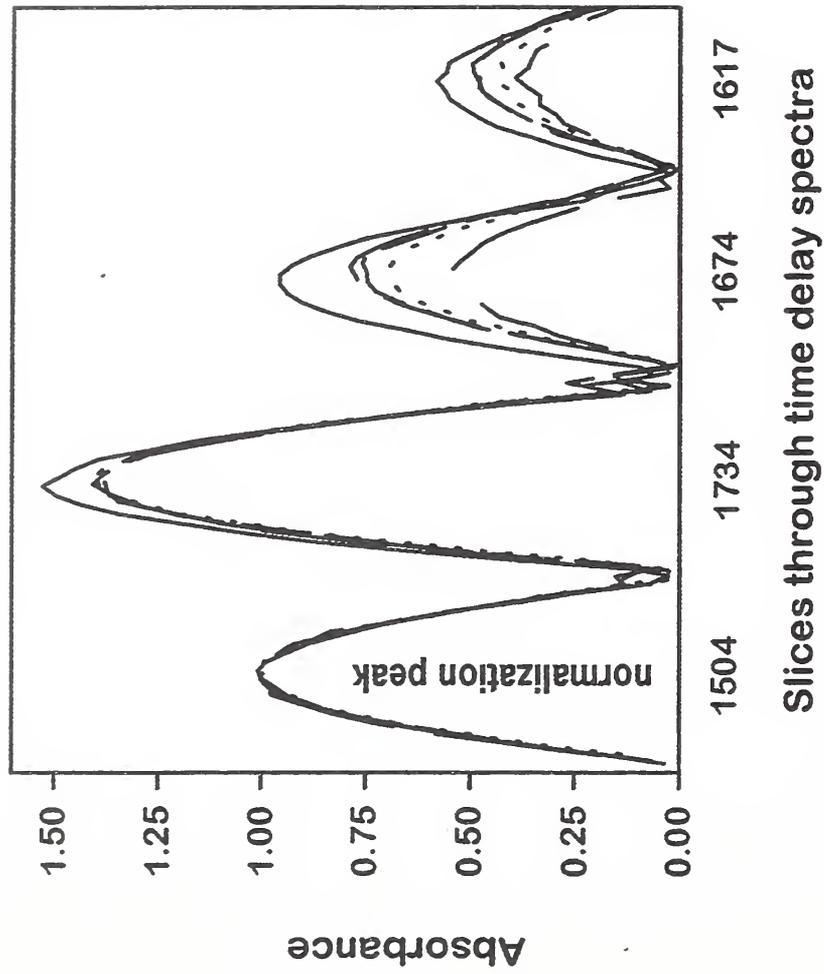
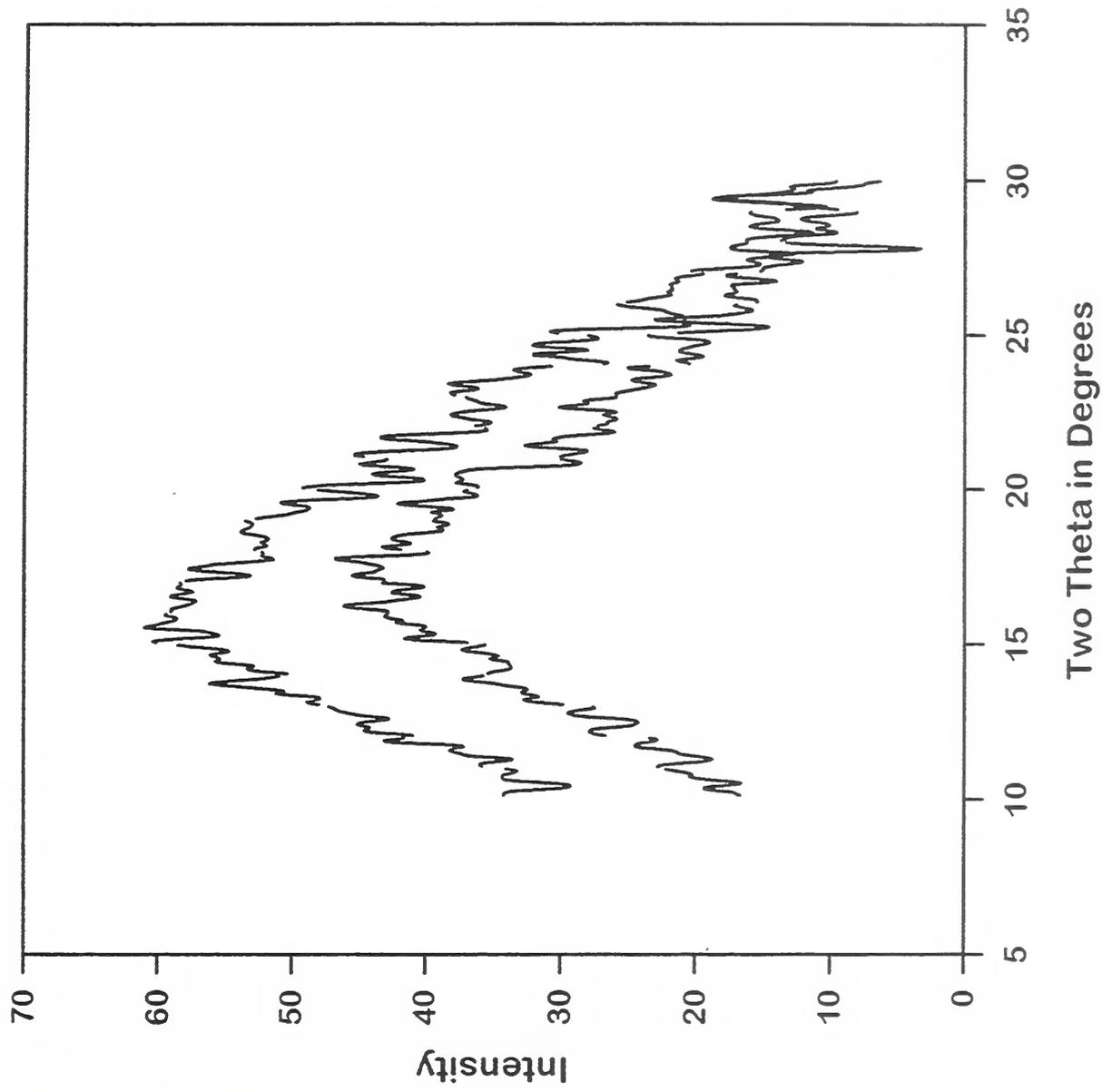Figure 16: Comparison of bilayer PA slices with PA slices from pure materials.

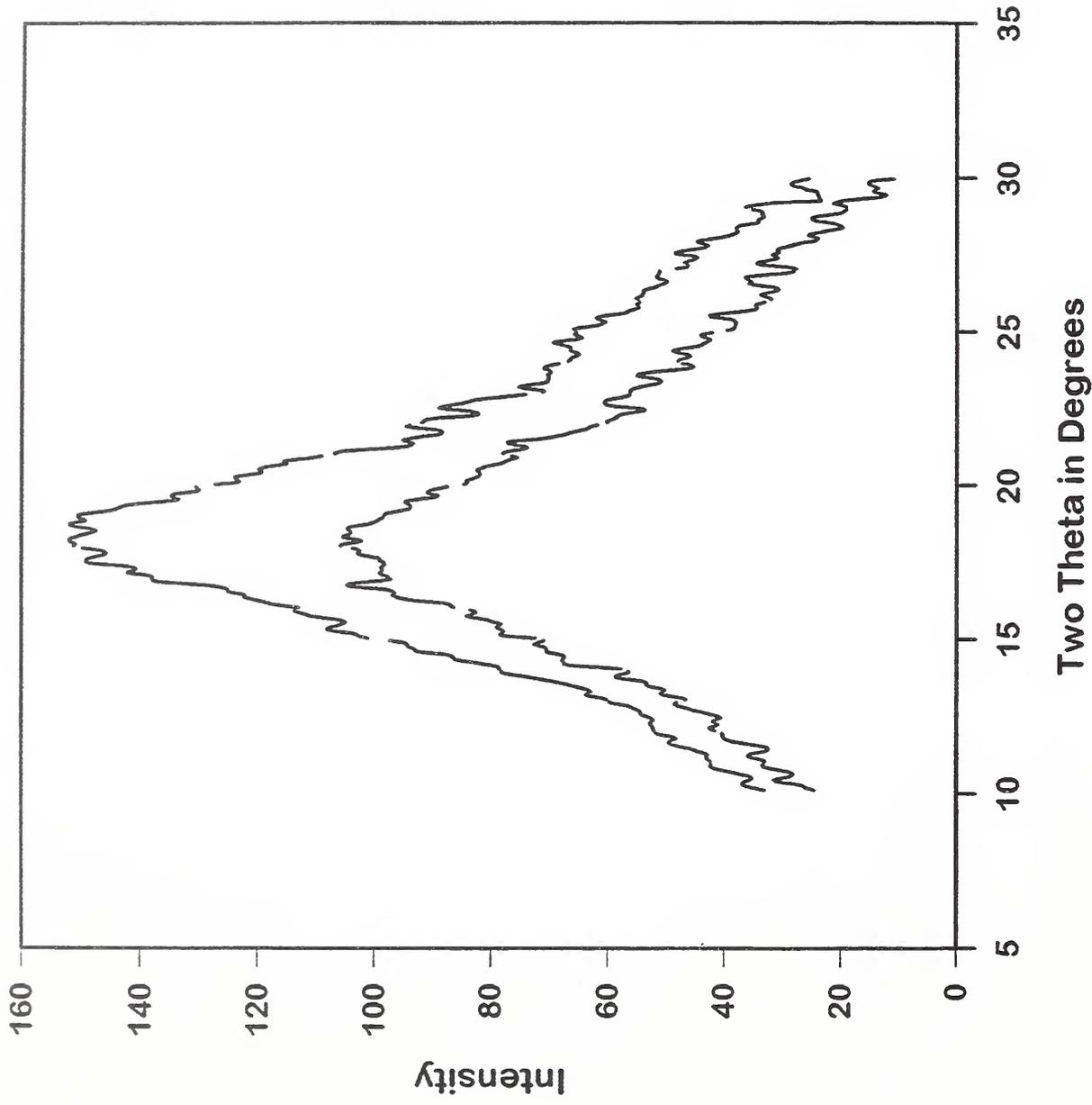Figure 17: X-ray Cu Kα diffraction from slowly (top) and rapidly (bottom) cured PI 2525 layer on glass.

Figure 18: X-ray Cu Kα diffraction from slowly (top) and rapidly (bottom) cured PI 2545 layer on glass.
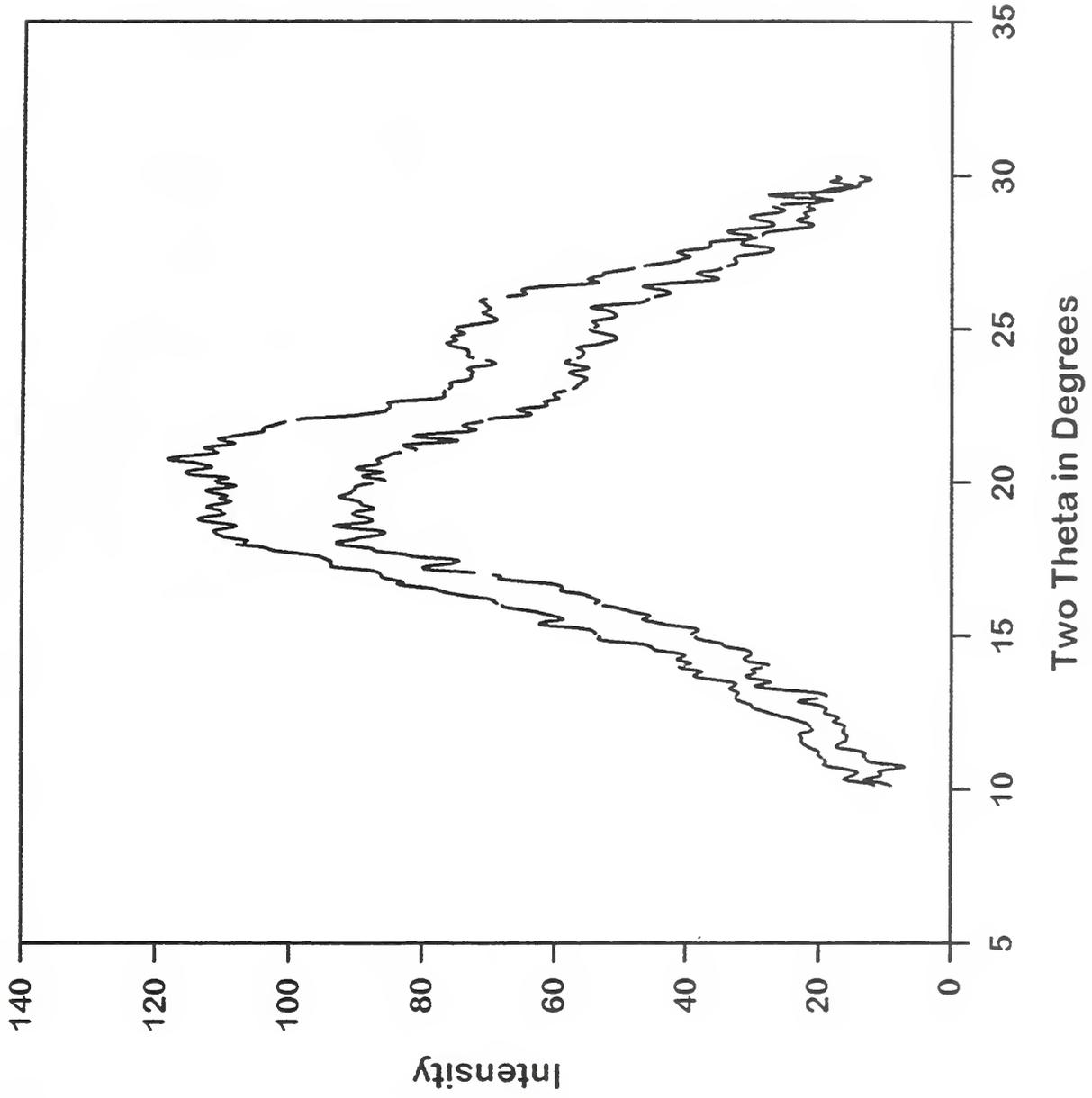
Figure 19: X-ray Cu Kα diffraction from slowly (top) and rapidly (bottom) cured PI 2611 layer on glass.